AD-A166 109

DNA-TR-85-121

U-SHAPED CURVE CONSTANT DETERMINED BY BARIUM RELEASE MEASUREMENTS

Clifford W. Prettie
Berkeley Research Associates, Inc.
P.O. Box 241
Berkeley, CA 94701-0241

DTIC
ELECTE
APR 1 0 1986
S D
D

5 April 1985

Technical Report

CONTRACT No. DNA 001-83-C-0080

Approved for public release;
distribution is unlimited.

THIS WORK WAS SPONSORED BY THE DEFENSE NUCLEAR AGENCY
UNDER RDT&E RMSS CODE B322083466 S99QMXBC00077 H2590D.

Prepared for
Director
DEFENSE NUCLEAR AGENCY
Washington, DC 20305-1000

DTIC FILE COPY

86 1 24 036

Destroy this report when it is no longer needed. Do not return to sender.

PLEASE NOTIFY THE DEFENSE NUCLEAR AGENCY, ATTN: STTI, WASHINGTON, DC 20305-1000, IF YOUR ADDRESS IS INCORRECT, IF YOU WISH IT DELETED FROM THE DISTRIBUTION LIST, OR IF THE ADDRESSEE IS NO LONGER EMPLOYED BY YOUR ORGANIZATION.

UNCLASSIFIED
SECURITY CLASSIFICATION OF THIS PAGE

AD-A166 107

REPORT DOCUMENTATION PAGE

Form Approved
OMB No. 0704-0188
Exp. Date: Jun 30, 1986

1a. REPORT SECURITY CLASSIFICATION UNCLASSIFIED	1b. RESTRICTIVE MARKINGS
2a. SECURITY CLASSIFICATION AUTHORITY N/A since Unclassified	3. DISTRIBUTION/AVAILABILITY OF REPORT Approved for public release; distribution is unlimited.
2b. DECLASSIFICATION/DOWNGRADING SCHEDULE N/A since Unclassified	
4. PERFORMING ORGANIZATION REPORT NUMBER(S) PD-BRA-84-320R	5. MONITORING ORGANIZATION REPORT NUMBER(S) DNA-TR-85-121
6a. NAME OF PERFORMING ORGANIZATION Berkeley Research Associates, Inc. 6b. OFFICE SYMBOL (If applicable)	7a. NAME OF MONITORING ORGANIZATION Director Defense Nuclear Agency
6c. ADDRESS (City, State, and ZIP Code) P.O. Box 241 Berkeley, CA 94701-0241	7b. ADDRESS (City, State, and ZIP Code) Washington, DC 20305-1000
8a. NAME OF FUNDING/SPONSORING ORGANIZATION 8b. OFFICE SYMBOL (If applicable)	9. PROCUREMENT INSTRUMENT IDENTIFICATION NUMBER DNA 001-83-C-0080
8c. ADDRESS (City, State, and ZIP Code)	10. SOURCE OF FUNDING NUMBERS PROGRAM ELEMENT NO. 62715H; PROJECT NO. S99QMXB; TASK NO. C; WORK UNIT ACCESSION NO. DH006620

11. TITLE (Include Security Classification)
U-SHAPED CURVE CONSTANT DETERMINED BY BARIUM RELEASE MEASUREMENTS

12. PERSONAL AUTHOR(S)
C.W. Prettie

13a. TYPE OF REPORT	13b. TIME COVERED	14. DATE OF REPORT (Year, Month, Day)	15. PAGE COUNT
Technical Report	FROM 840102 TO 840801	850405	86

16. SUPPLEMENTARY NOTATION
This work was sponsored by the Defense Nuclear Agency under RDT&E RMSS Code B322083466 S99QMXBC00077 H2590D.

17. COSATI CODES			18. SUBJECT TERMS (Continue on reverse if necessary and identify by block number)		
FIELD	GROUP	SUB-GROUP			
20	9		HANE	U-Shaped Curve	PLACES
20	6		Late-Time	Diffusion	Barium Cloud
			Striations	Ionospheric Conductivity	Conjugate Coupling

19. ABSTRACT (Continue on reverse if necessary and identify by block number)

The U-shaped curve has been suggested as a prescription for the size of late-time plasma structure. It is a specification of the structure size as normalized by a length parameter derived from the background ion-neutral slip speed and the effective cross-field diffusion constant. True to its name, the specification is a proportionality to a U-shaped function of the ratio between the integrated Pedersen conductivity of the magnetic field lines that have plasma structure on them and the integrated Pedersen conductivity of field lines in the background plasma (the M-ratio). The value of the proportionality constant in this relation, R, has been the subject of past analytical and numerical investigations. In this report experimental data from PLACES barium release JAN is investigated to derive an alternative value of R. Photographic, aircraft and rocket data sources are investigated to first determine the M-ratio, the diffusion constant and the characteristic structure sizes. The value of the proportionality constant R is then inferred.

20. DISTRIBUTION/AVAILABILITY OF ABSTRACT	21. ABSTRACT SECURITY CLASSIFICATION
☐ UNCLASSIFIED/UNLIMITED ☒ SAME AS RPT. ☐ DTIC USERS	UNCLASSIFIED
22a. NAME OF RESPONSIBLE INDIVIDUAL Betty L. Fox	22b. TELEPHONE (Include Area Code) 202/325-7042
	22c. OFFICE SYMBOL DNA/STTI

DD FORM 1473, 84 MAR 83 APR edition may be used until exhausted. All other editions are obsolete.

SECURITY CLASSIFICATION OF THIS PAGE
UNCLASSIFIED

20. ABSTRACT (continued)

From rocket data the integrated Pedersen conductivity of the background ionosphere is estimated to be less than 3.3 mho. From various souces of data but primarily aircraft phase data the integrated Pedersen conductivity of the JAN barium cloud is estimated to be more than 50 mho. These values imply an M-ratio of more than 15. The dynamics of the cloud derived from optical data suggest an M-ratio of no more than 5. Coupling to the southern conjugate may provide the additional background conductivity to explain the discrepancy. Coupling to the conjugate is size dependent and may provide an additional structure size selection mechanism.

The structure sizes observed in JAN are well characterized by a range of values centered near a 280 meter diameter. The corresponding breakpoint wavenumber is found to be 90 meters. Optical and aircraft data both provide size estimates close to this value. The rocket data is not in disagreement with it.

The density profiles measured by the rocket data have steep gradients with gradient lengths as small as 18 meters. A novel analysis of one of these gradient profiles reveals the diffusion constant to be roughly 3 meters squared per second. The plasma diffusion mechanism is suggested to be electron-neutral collisions.

The value of R obtained from the JAN data is significantly larger than that suggested by numerical studies. The discrepancy suggests the possible role of alternative size selection mechanisms or yet other explanations.

TABLE OF CONTENTS

QUALITY INSPECTED 8

Availability Codes
Dist Avail and/or Special
A-1

LIST OF ILLUSTRATIONS

LIST OF ILLUSTRATIONS (continued)

LIST OF TABLES

SECTION 1

INTRODUCTION

The U-shaped curve, Figure 1, has been suggested as a prescription for plasma structure size in the late-time high altitude nuclear explosion (HANE) environment. The curve specifies a structure size, L, in terms of the diffusion coefficient transverse to the magnetic field, D, and the relative speed, U, of the neutral wind through the background plasma, as:

$$\frac{LU}{D} = R \frac{(M+1)^2}{M-1} \qquad (1)$$

In this relation M represents a ratio which can be obtained from the field line integral of the (transverse) Pedersen conductivity. The ratio between the maximum and minimum field line integrated conductivity values is defined as M in the ideal case in which the conductivity parallel to a field line is assumed infinite. For situations in which infinite parallel conductivity is not the case the value of M remains to be fully clarified. From a current understanding of the physics it is expected that in these situations an effective value for M could be defined for use in a structure size prescription like equation 1.

The term, R, in equation 1 represents a dimensionless constant whose value has been suggested to range from 1/2 to 100 by numerical and analytical investigations of the gradient drift mechanism (Zalesak and Huba, 1984). This wide range in possible values which results from the models implies a correspondingly wide range of possible structure sizes.

The wide range of structure sizes is made even wider by uncertainties in the value of the transverse plasma diffusion constant, D. The classical value for the plasma transverse diffusion is controlled by the electron diffusion rate.

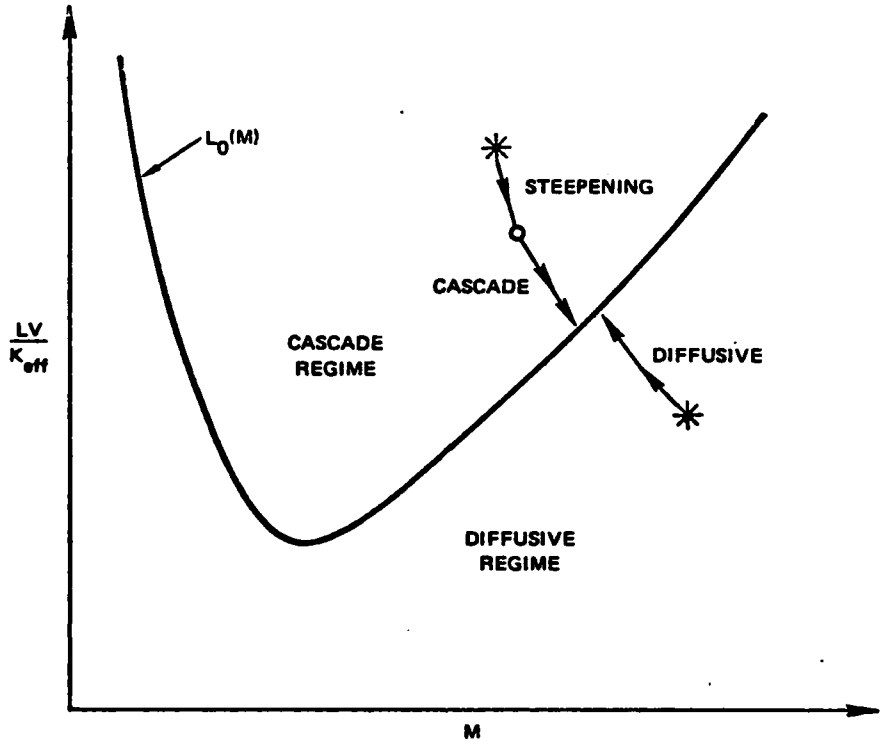

FIGURE IV-6 STRUCTURE EVOLUTION MODEL PROPOSED BY WITTWER

Figure 1. The U-shaped curve prescription for structure size, L. (From a summer study report.)

This value is very much smaller than the ion transverse diffusion rate. Under certain situations (Francis and Perkins, 1975) in which the structured plasma electrostatically couples to other regions of the ionosphere which are smooth or structured in a different manner, the rate of plasma diffusion may proceed at a rate which is a substantial fraction of the ion rate implying a much larger value for D. These considerations broaden the (already too broad) range of predicted structure sizes by a factor of possibly more than 100.

It is the purpose of this report to discuss an investigation of experimental data which evaluates the constant R. In the investigation, the transverse diffusion mechanism and the coefficient, D, have also been identified providing experimental evidence which allows a significant narrowing of the range of the prescribed structure sizes.

The source of the data for the investigation is measurements made during the PLACES barium release, JAN. The dynamics of barium plasma clouds are controlled by the same physics that controls late-time HANE structures and they consequently serve as excellent objects for testing structure models. The JAN release produced a well structured barium cloud which was well diagnosed. During JAN a rocket payload was flown through the barium plasma. The payload measured electron density as well as ionic constituents and is a good data source. The JAN barium cloud also drifted in a direction such that photography of its structure transverse to the magnetic field could be obtained providing optical data on structure size and morphology. Measurements of propagation effects on a UHF satellite-to-aircraft signal link are also available and prove to be valuable.

The investigation is presented in this report in several major sections. The next section discusses a derivation of the M-ratio determined from the data. Several subsections

therein discuss evaluations of the ion mobility, the background conductivity, the ion cloud conductivity and an alternative conductivity ratio estimate. Evidence is found for electrostatic coupling to the conjugate ionosphere which is also discussed.

Section 3 is a brief section which presents estimates of the structure size, L, obtained from various experimental sources of data.

In Section 4 the diffusion effects are considered. Measurements of the gradient length of steepened structures is presented. The diffusion coefficient and mechanism is also determined with what is believed to be a novel but nevertheless straightforward technique.

In Section 5 results and conclusions are presented. The value of R determined by the experimental measurements is presented and then compared with numerically determined values for R. Conclusions are then drawn.

SECTION 2

THE M-RATIO

The M-ratio which enters the U-shaped curve relation is defined in the Introduction as the peak-to-background ratio of the field-line integrated Pedersen conductivity. The local Pedersen conductivity is given by

$$\sigma_P = \frac{e \mu N}{1 + (\mu B)^2} \qquad (2)$$

Where N is the local ion density, μ is the local ion mobility, B is the magnitude of the magnetic field, and e is the charge of the ion. The field line integrated conductivity is the integral of this quantity with respect to distance along a field line. Frequently it is more convenient to discuss the height integrated Pedersen conductivity which is related by a factor of the cosine of the 60° dip angle to the field line integrated value.

With the JAN rocket data it is possible to evaluate the integrated conductivity of the background ionosphere below 240 kilometers and to estimate its value for the entire background ionosphere. The first two subsections present this estimate. Section 2.1 presents a discussion of the evaluation of the mobilities of various ion species in the background gas mixture while Section 2.2 combines these results with the rocket data to produce the estimate.

Evaluation of the M-ratio is possible with the results of Section 2.3 which provide an estimate for the integrated Pedersen conductivity of the barium cloud. The value found for the M-ratio is significantly different from the M-ratio determined from the photographic measurements of cloud dynamics as is discussed in Section 2.4. This discrepancy provides evidence for coupling to the conjugate F-region and is discussed in Section 2.5. Section 2.6 suggests that conjugate coupling may play a role in the size selection mechanism.

2.1 MOBILITY VALUES

In this section the mobility of barium, normalized to the magnetic field magnitude B, is first evaluated. Mobility values for air ions are derived next. A comparison with other published values is then presented.

The barium mobility has been determined through a straightforward scaling of an experimental value presented graphically in Brown (1958) and discussed in Linson (1970). The value presented in Brown (1958) is for barium ions in a neutral gas of N_2 at one atmosphere (see Figure 2). The scaling to ionospheric neutral densities goes according to number density (Linson, 1970) yielding for the μB factor the value

$$\mu B = \frac{2.7 \times 10^{17}}{N} \tag{3}$$

Intermediate quantities used to obtain this value are:

$\mu = 2.3 \times 10^{-4}$ m^2/volt-sec at 1 atm at 273°K

1 atm = 760 torr

1 torr = 133.322 newtons/m^2

N at 1 atmosphere 273°K = $2.688 \times 10^{25}/m^3$

$B = .45 \times 10^{-4}$ Tesla

In expression (3) the term N represents the equivalent N_2 neutral particle number density which may not correspond to the particle number density of the neutral air. The mobility of an ion does have a dependence upon the mass of the neutral gas particles, M_g, which according to Brown (1958, eq. 3.16) is

$$\mu \propto (1 + M_g/M_i)^{1/2} \tag{4}$$

where M_i is the mass of the ion particles. For barium ions this dependence implies negligible differences among the primary neutral constituents at 100-300 km altitudes. For barium ions the term N is, thus, well approximated as the

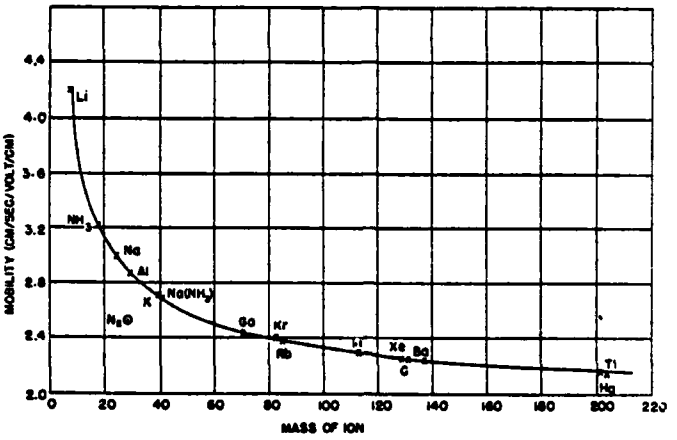

Fig. 3.20. Mobility in nitrogen of various ions as a function of mass at 1 atmosphere pressure.

J. H. Mitchell and K. E. W. Ridler, Proc. Roy. Soc. (London) A146, 911 (1934).

Figure 2. The mobility of various ions in nitrogen. (From Brown 1958, p. 62.)

number density of the neutral air. (This differs from Linson's (1970) work but produces at most a 25% difference in mobility for Ba^+ in pure neutral oxygen.)

The mobilities of the background ions, NO^+ and O^+, in pure N_2 has been determined by scaling the Ba^+ mobility according to the mass related factor given by relation 4. This scaling ignores the ion size-related cross-sectional differences but should prove adequate for the purposes of this report. In adjusting the derived values to account for a neutral gas mixture instead of neutrals of pure N_2, the neutral gas mass dependence of equation 4 now plays a significant role since the ion mass is much less. In calculating the equivalent pure N_2 neutral number density for O^+ another consideration must be made; namely, that the mobility of O^+ in O is probably less than the scaling relation would indicate because of the likeness of the ion and neutral species (see N_2^+ in Figure 2). The resulting relations for the μB factor have been chosen as:

$$\mu B_{NO^+} = \frac{2.7 \times 10^{17}}{\frac{N_2 + O_2}{1.3} + \frac{O}{1.1}} \qquad (5)$$

$$\mu B_{O^+} = \frac{2.7 \times 10^{17}}{\frac{N_2 + O_2}{1.5} + \frac{O}{1.3}}$$

where the symbols N_2, O_2 and O above represent the number density (in particles per cubic meter) of the gases N_2, O_2 and O, and where the O^+ mobility expression assumes that in a background of neutral atomic oxygen its mobility is 90% less than the mass scaling relation would indicate. Using values for neutral constituents tabulated in the U.S. Standard Atmosphere (1976) the mobility values of Ba^+ and O^+ are plotted in Figure 3.

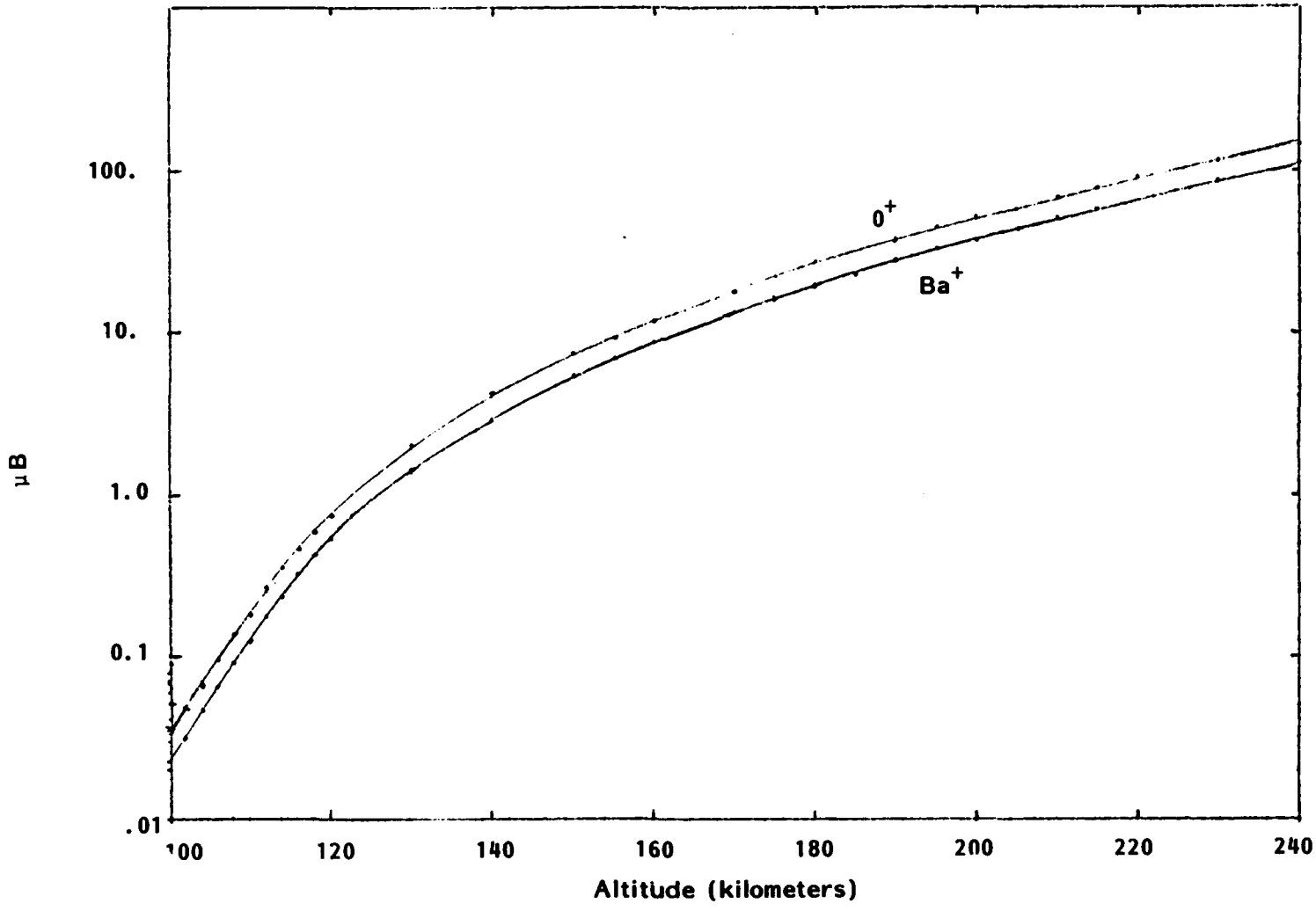

Figure 3. Mobility values vs altitude for Ba^+ and 0^+. (Values for NO^+ lie near geometric mean.)

The computed values of μB can be compared with values published by others (Table 1). Linson (1970) lists a value of 7 for μB at 150 kilometer altitude which is somewhat higher than the 5.2 value calculated by the above relations. The discrepancy may be associated with rounding error in that Linson (1970) defines the collision time to one significant figure, i.e.,

$$\tau_i = \frac{9 \times 10^9}{N(in/cc)} \tag{6}$$

and then obtains further results from this benchmarking relation.

Hochstim (1970) presents model results for ion-neutral collision frequencies in the ambient atmosphere. At altitudes of 150 km and 160 km collision frequencies of 3.3 and 2.5 per second are predicted. The implied μB factors for NO^+ ions are 43.6 and 57.6 respectively. These values are somewhat larger than the values of 6.4 and 10.4 predicted by the above relations.

Simons et al. (1984) in Appendix D present a calculation of the Pedersen conductivity of the background ionosphere prior to PLACES event GAIL. Their μB values are derived from a collision frequency model referenced as that of Banks and Kocharts (1973). Using their Figures D-3 and D-4 the conductivity (6.2×10^5 stat mhos/cm) and the electron density (7×10^4/cc) at 160 kilometers can be used to evaluate the μB ratio assumed. This value is found to be 3.3 and is thus lower than that predicted by the relations herein. However, Dupré's (1984) addendum to this work revises this figure upward to a value of 10. This value is in good agreement with the values predicted by relation (5).

Kilb (1977) presents a relation for the ion neutral collision frequency for barium and air ions in a background

Table 1. Comparison of calculated μB with different published values.

	μB Ba	μB NO^+	
Altitude in kilometers	150	150	160
Simons et al. (1984)*	-	-	10.
Relations (3) and (5)	5.2	6.4	10.4
Kilb (1979)	6.5	2.8	4.6
Linson (1970)	7.0	-	-
Hochstim (1970)	-	43.6	57.6

* As modified by telephone discussions with Dupré (6/84)

of air. The relation specifies the collision frequency as a simple proportionality to mass density (not inverse number density in contrast with (3) and (6)). The value of μB determined from the relation is 6.5 for barium at 150 kilometers. For air ions (28 a.m.u.) mobility values are found to be 2.8 and 4.6 at 150 and 160 respectively. The barium ion value is notably in good agreement with the relation (3) despite its simplicity and its questionable proportionality relation. The air ion mobility values are considerably lower than those predicted by relation (5) although little weight should probably be given to this discrepancy due to the approximate nature of the relation in Kilb (1977).

The comparisons discussed above are summarized in Table 1. In general the relations used herein produce μB values in good agreement with those of Simons et al., as amended by Dupré (1984); lower values than would be inferred from Hochstim (1970) and values very similar to those predicted by Linson (1970). The agreement with Linson (1970) values should not be overly surprising since the approach taken herein closely parallels his.

2.2 PEDERSEN CONDUCTIVITY OF THE BACKGROUND IONOSPHERE

Figures 4 and 5, reproduced from Narcisi (1981), show the results of the ion mass spectrometer experiment which performed rocket-borne measurements of the ionosphere during JAN. From these measurements and the mobility results of Section 2.1 an estimate of the field line integrated Pedersen conductivity of the background ionosphere may be made, as is presented in this Section.

Figure 4 shows the measured ion composition versus altitude and provides a clear indication that the rocket payload passed through the barium cloud. Figure 5 shows

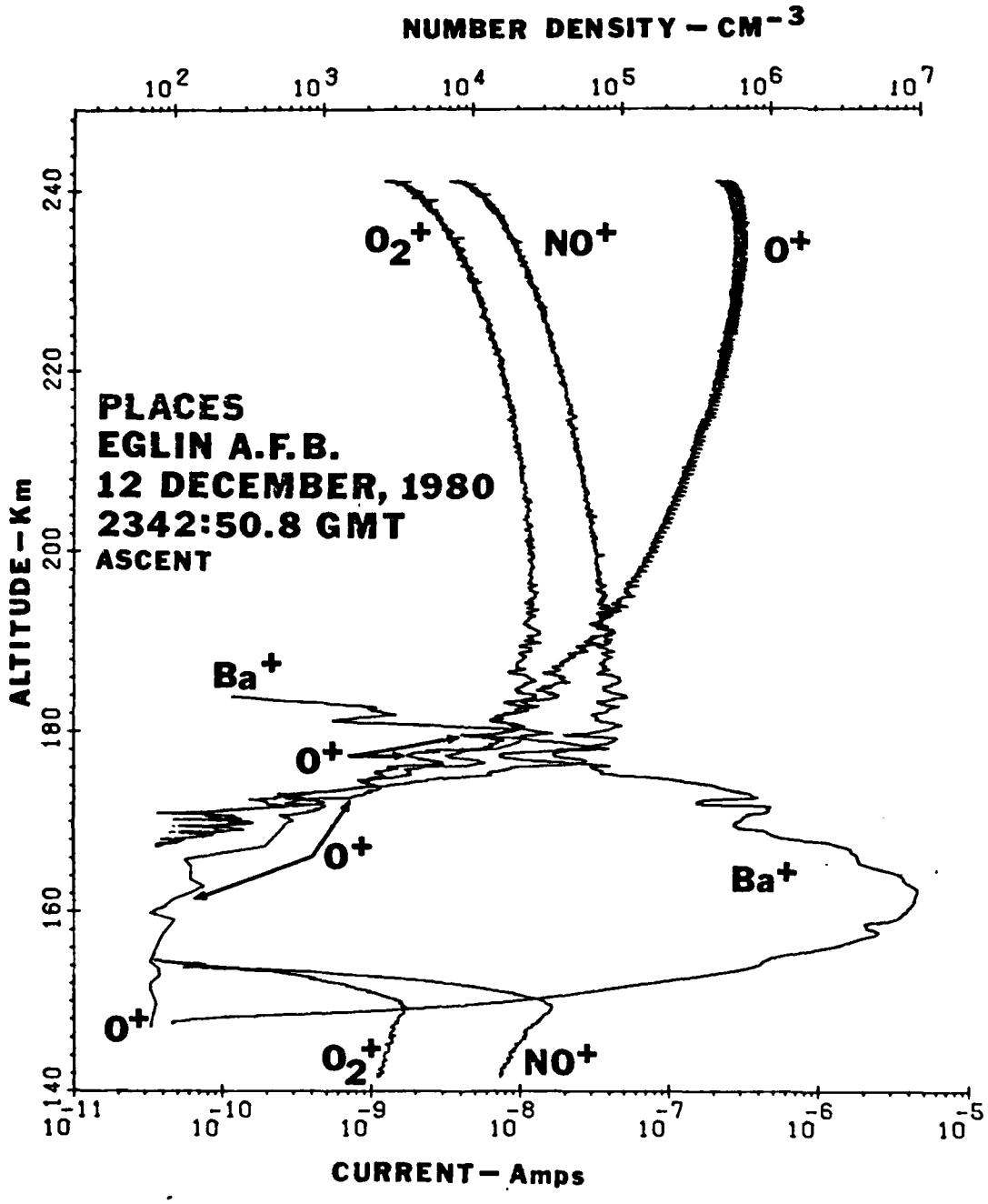

ASCENT MEASUREMENTS SHOWING THE PENETRATION OF THE BARIUM CLOUD AND ITS EFFECTS ON THE NORMAL AMBIENT SPECIES NO^+, O_2^+, AND O^+

Figure 4. Ion density measurements during JAN. (From Narcisi et al., 1981.)

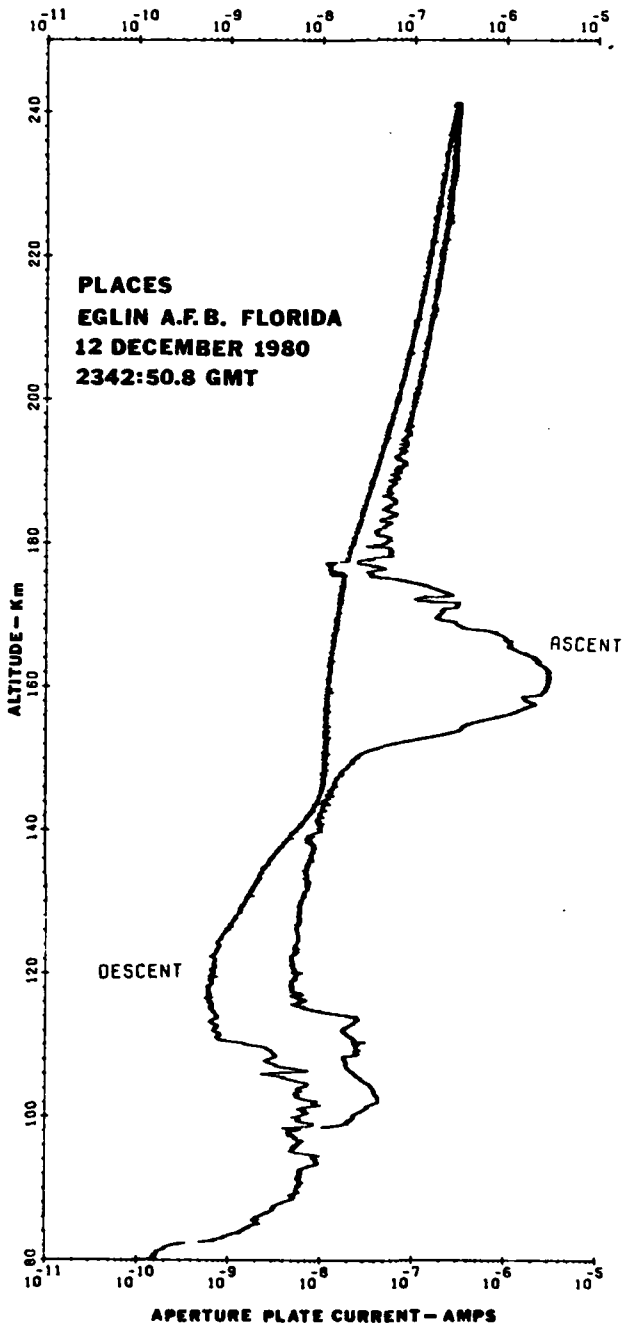

AN EXPANDED PLOT OF THE ASCENT AND DESCENT APERTURE PLATE CURRENT MEASUREMENTS IN THE VICINITY OF THE BARIUM CLOUD

Figure 5. Plasma density measurements during JAN. (From Narcisi et al., 1981.)

the total current measured by the spectrometer and while it does not convey any information regarding ion species it is useful because it extends the altitude range over which density measurements are available.

In Figure 5 a clearly defined region of enhanced density is indicated to exist between 100 and 116 kilometers altitude on the upleg. A similar region with significantly lower density is also indicated on the downleg. This difference in density between the upleg and downleg regions is intriguing because it is suggestive of an image effect. From the gross trajectory geometry the upleg region is very nearly directly below the barium cloud on the field lines whereas the corresponding region on the downleg is a great distance away. If the electrostatic field of the cloud were capable of influencing these lower altitude regions (see Section 2.5) then an enhancement of the local density similar to that seen in Figure 5 could be produced. This evidence for image effects is tenuous, however, as an equally appropriate explanation exists that the difference is merely the result of horizontal variations in the background ionosphere which are unrelated to the ion cloud presence.

The ion density of the background ionosphere has been determined from the values shown in Figures 4 and 5 and is shown plotted in Figure 6. In reading values from Figure 5 the current to density scale factor of 2.1×10^{12} indicated by the dual abscissa scales of Figure 4 has been used for consistency. Figure 4 has been used whenever possible to obtain density values by species. Use of the Figure 4 values is inappropriate for determining background values in the 150-175 kilometer altitude region occupied by the barium cloud so downleg values from Figure 5 are used for this region. Since the downleg values are consistently less, they were scaled up from the plotted values by a factor

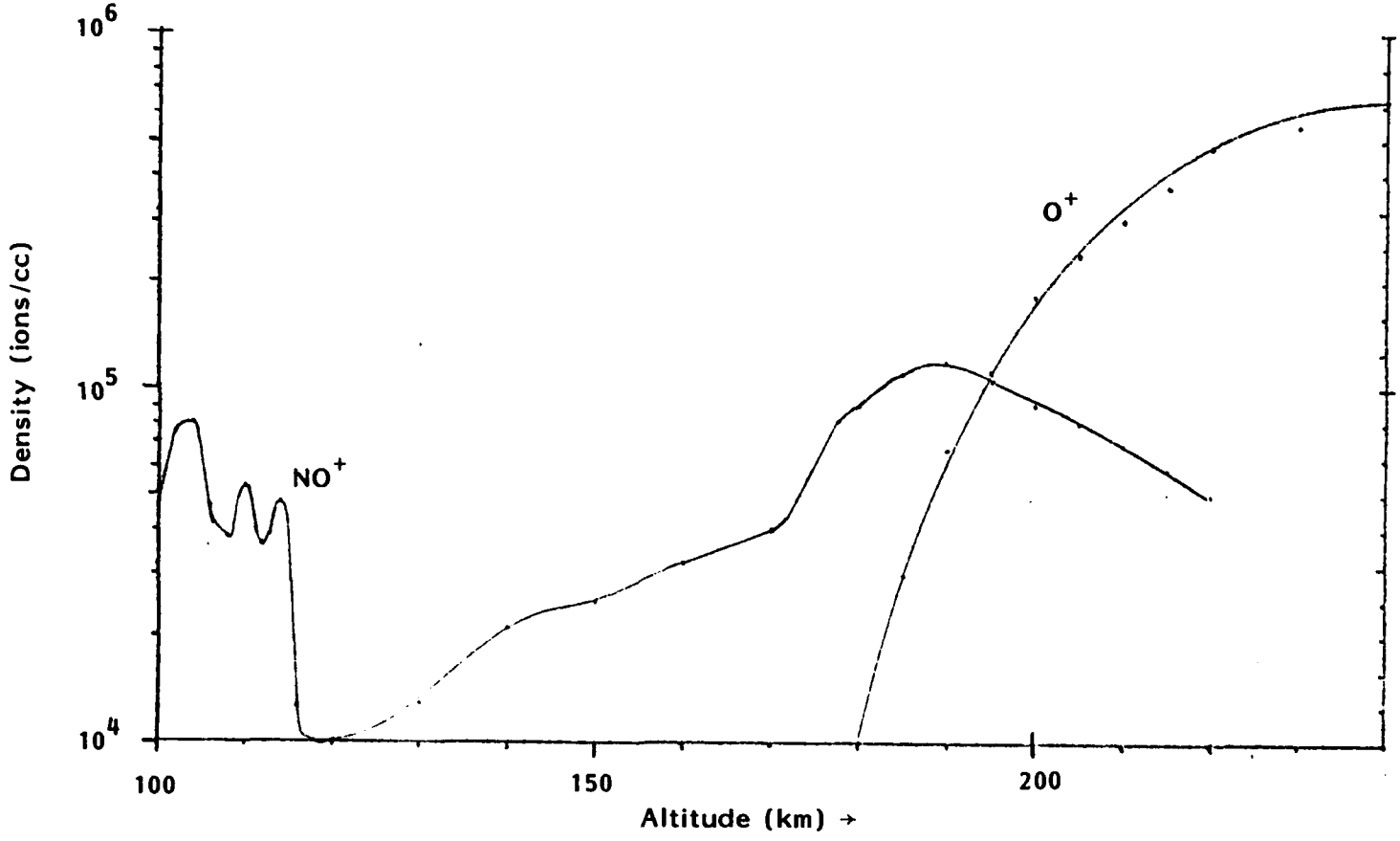

Figure 6. Ion density of background ionosphere from JAN mass spectrometer rocket payload. (Obtained from results of Narcisi et al. (1981).)

of 1.2 in obtaining values for Figure 6. Values for density below 140 kilometers must also be taken from Figure 5 and in this case upleg values are used. The species is assumed to be NO^+ for the entire measurement region below 140 kilometers.

Using the density values of Figure 6 and mobility values of Figure 2 the Pedersen conductivity of the background ionosphere has been calculated and plotted in Figure 7. Plot values represent

$$\frac{\mu BN}{1 + (\mu B)^2} \tag{7}$$

in units of 10^{10} per m^3 and the Pedersen conductivity, which is e/B times this quantity, may be obtained by scaling with the factor .0355 m^3 mho/km.

The height integrated Pedersen conductivity of the background has been evaluated by integrating the curve in Figure 7. The integrations have been performed over the regions noted in Table 2 which roughly correspond to E-region, ionospheric background near the cloud and the F-region up to 240 km. The conductivity of the F-region above 240 kilometers altitude has also been estimated by assuming that it has a constant density of 1.1×10^6 and a neutral density scale height of 30 kilometers. The resulting value should represent an overestimate of the conductivity because measurements by Gonzalez (1981) prior to event GAIL indicate a comparable value as the peak F-region density at a time 1/2 hour earlier. The total height integrated Pedersen conductivity indicated by the table is 3.3 mho. This value is in good agreement with the 3.5 mho value quoted in Francis and Perkins (1975) for the twilight ionosphere.

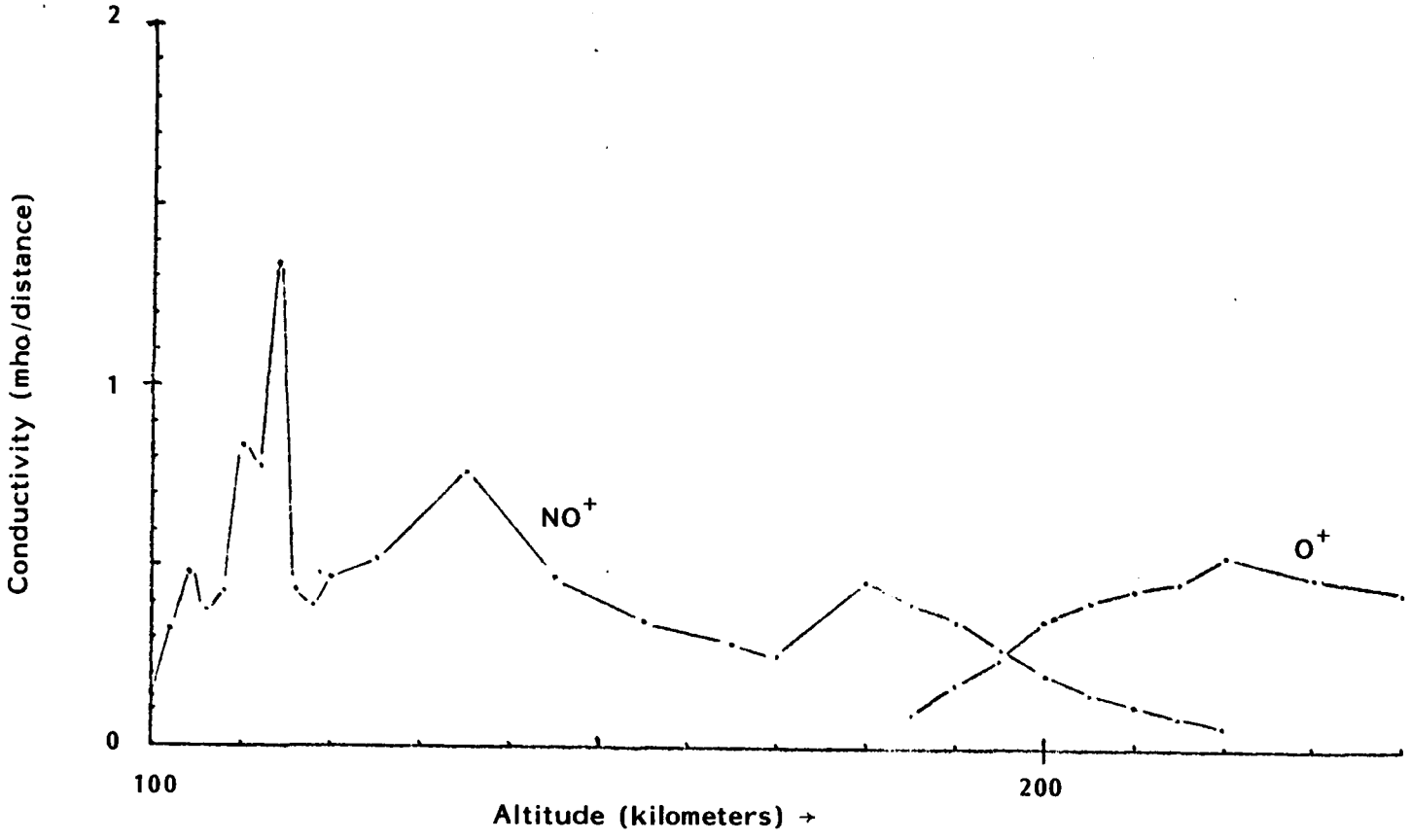

Figure 7. Conductivity vs Altitude from JAN mass spectrometer data. To convert from ordinate values to mho/km multiply by .0355.

Table 2. Pedersen conductivity values for JAN.

Altitude	Background Conductivity in mhos
100-120	.4
120-170	.9
170-240	1.2
240-Equator (Estimate)	.8
TOTAL	3.3

2.3 INTEGRATED PEDERSEN CONDUCTIVITY OF THE CLOUD

In this section the integrated Pedersen conductivity of the cloud is estimated using results from the rocket experiment, satellite-to-aircraft signal measurements, and theoretical models of cloud morphology.

The barium ion density measurements of Figure 4 indicate that the barium profile is centered at 162 kilometers and that it is localized to an e-folding altitude range of ±5.2 kilometers. Use of this fact is made to simplify the estimate of cloud conductivity by assuming that the average μB factor is 10, i.e., the μB value indicated for Ba^+ at 162 kilometers by the mobility curve of Figure 2. With this approximation the integrated conductivity values are straightforwardly expressed in terms of the more easily estimated integrated particle content values.

Table 3 summarizes the values for the integrated cloud conductivity from various sources of data and data models.

From the previously mentioned e-folding radius and the peak density of 9×10^6 indicated by the rocket data (Figure 4) a value for the height integrated ion content of $8.3 \times 10^{16}/m^2$ is found. This value implies a height integrated conductivity of 29 mhos and should be regarded as a lower bound. The rocket trajectory may not have passed through the region with peak ion density or may have passed through the cloud with a significant component across it. In either case the integrated conductivity which results would be lower than the actual value.

Measurements of the phase shift of the satellite-to-aircraft signal are straightforwardly related to the electron content integrated along the line-of-sight (LOS). The LOS integrated content implied by the data at the time of the rocket is 7×10^{16} per square meter (Marshall, et al. 1982) which implies an LOS integrated conductivity of 25 mhos.

Table 3. Estimates of integrated content and conductivity of JAN at 30 minutes after release.

	Height Integrated Content $\times 10^{-16}$ m^2	Conductivity μB = 10 mhos
Rocket	8.3	29
Aircraft (LOS integrated)	7	25
Aircraft	15	53*
Theory	21	73

* Best conservative estimate

The relation between the phase data from the aircraft and the height integrated conductivity is not as straightforward. A geometric model of the cloud and the propagation path must be formulated to convert the LOS integrated values to field line integrated and height integrated values. From the known satellite azimuth and the elevation of 210° and 38° respectively (Marshall et al. 1981) the line-of-sight can be found to intersect the barium cloud field lines at an angle of approximately 30°. From the results of Linson and Baxter (1977, p. 75 Model B as specified by Linson, 1984) the JAN density contours may be estimated as ellipses elongated along the magnetic field with a 7-to-1 major-to-minor axis ratio. Under this assumed geometry the height integrated cloud conductivity may be found to be 53 mhos.

From a theoretical standpoint the peak height integrated electron content should remain constant (Linson and Baxter, 1977) until bifurcation permits diffusion to become effective or until the Pedersen convection of background ions (Prettie, 1982) into the cloud can cause significant decay. The peak initial value of the field line integrated content should be roughly 2.4×10^{17} electrons per square meter (Linson and Baxter, 1977, p. 75, Model B per Linson, 1984) which would imply a peak integrated Pedersen conductivity of 73 mhos. This value is somewhat larger than that derived from the aircraft data.

In the next section it is seen that the M-ratio found from the rocket data is much larger than that found from photographic data--a result with significant implication to be discussed later. With this foresight it is conservative to choose a value for the cloud conductivity that is on the low side. A value of 50 mhos for JAN is in line with the aircraft data and is believed to represent a best conservative estimate of its integrated Pedersen conductivity. Actual values as high as 75 mhos might realistically apply. Values

much lower than 50 mhos, however, would be difficult to argue for. With this value and the background conductivity value of 3.3 mhos found in the previous section an M-ratio of 15 is implied.

2.4 THE M-RATIO IMPLIED BY PHOTOGRAPHIC MEASUREMENTS

Because the dynamics of the plasma cloud are strongly influenced by the M-ratio, they can be used as a diagnostic of its value. Photographic measurements of the ion cloud and neutral cloud positions can be used to determine the average motion of both the ambient and high density plasma regions with respect to the neutrals. These quantities may then be used to estimate the M-ratio. This technique has been applied to barium data in the past by Linson and Baxter (1977) and in this section it is applied to photographic data from JAN.

A photograph of the JAN barium cloud taken at 23 31:08 or 17 minutes after release has been provided by Wallace Boquist of Technology International Corporation. The photograph is of the cloud as viewed from site A-105 which fortuitously was in a position such that the cloud was nearly at the magnetic zenith. Figure 8 shows a tracing of the relevant features of the photograph. Distances on the tracing can be used to estimate the coupling factor defined by Linson (1972). Since the distance between the low density and high density barium ions is 2/3 of the distance between the low density barium ions and the center of the neutral cloud a coupling factor, η, of .67 is implied.

The coupling factor is related to the M-ratio using analytical expressions for simplified models of the cloud. Zalesak and Huba (1984) present the following expression for the speed of the peak density region of an elliptical constant density conductive plasma in terms of its M-ratio:

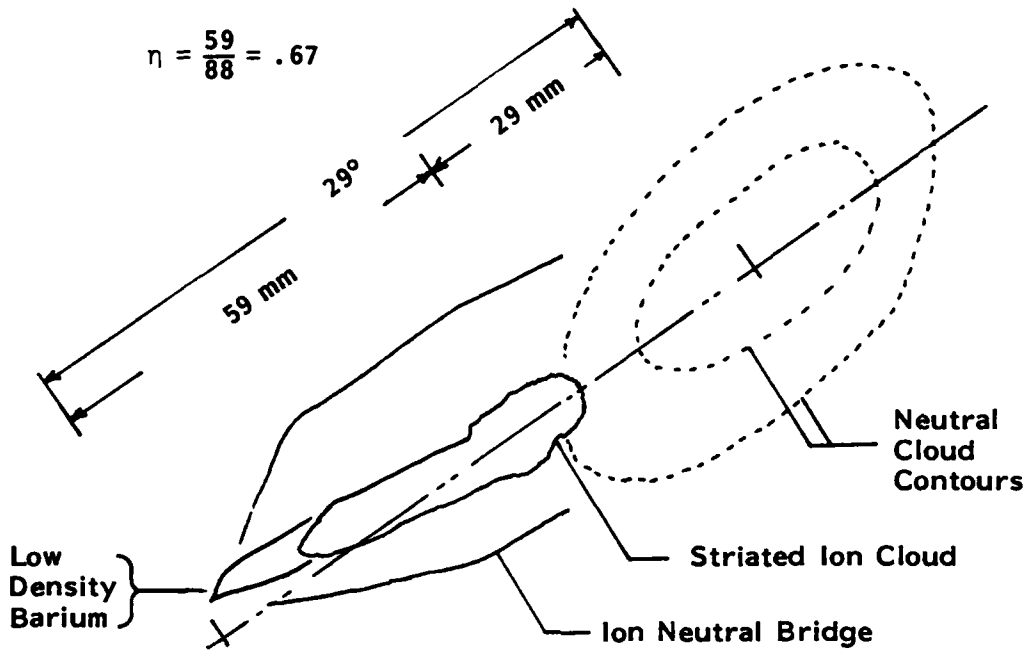

Figure 8. Tracing of photograph of JAN taken at 23 31:08 from site A-105 (photograph provided by Wallace P. Boquist, Technology International Corporation).

$$v_i = v_o \frac{1 + R}{1 + MR} \tag{8}$$

where v_i is the speed of the elliptical cloud, v_o is the speed of the exterior plasma, R is the ratio of the major to minor axis, the ellipse is assumed elongated in the direction of the cloud motion, and the neutral fluid is assumed to be everywhere stationary. The value for the M-ratio implied from the coupling factor, η, by the above relation is:

$$M = \frac{\eta/R + 1}{1 - \eta} \tag{9}$$

Table 4 lists the M-ratio implied by a coupling factor of .67 (as well as .6 and .75) and various values of R. These ratios lie between 5.1 and 3.1

Narrowing down this range of values would be possible if a value of R could be determined. The ellipticity of the cloud indicated in the tracing is roughly of order 2 and provides a rough guess for R. Identifying a value much better than this rough guess seems difficult. Individual striations that are not shown in the tracing but that are apparent in the picture may have an ellipticity as large as 100. On the other hand, the peak density profiles of the main cloud and of the striations themselves may not be elongated as indicated by the photographic outlines of the cloud because the significant brightness of low density barium may mask the true shape of the higher density barium contours which control the dynamics. As a further factor, the photographically derived coupling factor is essentially averaged over the lifetime of the cloud. A lifetime averaged ellipticity factor should be used arguing for M-ratios from R values lower than those apparent. Because of these various

Table 4. M-ratios implied by various coupling factors, η, and various ellipticity factors, R.

R	η = .6	η = .67	η = .75
1	4.0	5.1	7.0
2	3.3	4.0	5.5
5	2.8	3.4	4.6
10	2.7	3.2	4.3
100	2.5	3.1	4.0

factors it is difficult to significantly narrow the range of implied effective (lifetime averaged) M-ratios.

Despite the variation in values of photographically derived M-ratios, the existence of a gross discrepancy with the M-ratio of 15 derived from the rocket data cannot be denied. This discrepancy is significant and is addressed in the next section.

2.5 COUPLING CONSIDERATIONS

Photographic measurements suggest that the M-ratio of the cloud lies between 3.1 and 5.1. Rocket measurements of the local ionosphere and aircraft measurements of the cloud integrated content suggest an M-ratio of no lower than 15. Similar results have been obtained from similar comparisons in the past (Linson 1972) and have been explained through conjugate coupling.

Coupling to the conjugate ionosphere also seems to be a possible explanation for the JAN data. The conjugate ionosphere at 53°S and 101°W is daylit and should be capable of providing the 7 mhos needed to bring the M-ratio values into agreement. The primary impediment to conjugate coupling is the resistivity of the plasma parallel to the field. This resistivity, however, is predicted to be small enough that, in spite of the large distances involved, the large-scale variations in the electrostatic potential produced by the cloud will be felt by the conjugate region.

Assuming an intervening plasma temperature of 2000°K the electronic mobility may be found from classical collisional considerations to imply that a 1 km radius region couples through the 18,900 kilometer distance to the conjugate ionosphere with .1 ohms of resistance. This low resistance may allow significant coupling currents to develop. Note,

however, that smaller scale structures in the potential effectively see a higher resistance in indirect proportion to their area transverse to the field. Structures smaller than 300 meters experience more than 1 ohm coupling resistance and, consequently, probably don't couple effectively.

The second impediment to coupling is the bleeding off of parallel currents by Pedersen currents across the field. However, since the Pedersen conductivity is very low above the F-region peak the upper ionosphere is an effective insulator in the transverse dimension and this consideration is not as important as the first for larger sized structures. Its major role seems to be in limiting coupling to the E-region below the cloud.

A more quantitative description of the coupling process is possible by considering the root of the ratio of the parallel to perpendicular conductivity. This ratio gives the scaling which when applied to the 3-dimensional potential problem can be used to convert parallel-to-the-field distances from actual distances to those appropriate for an isotropically but spatially varying conductor. This factor is tabulated as a function of altitude in Table 5.

Also tabulated is the effective distance of an altitude region from a disturbance in the potential at 160 kilometers which is found by applying the scaling factor. The implication of the results in this latter column is that the local E-region below 120 kilometers altitude is effectively further away than the conjugate F-region. It is only fair to note, however, that the conjugate F-region is effectively separated by a region of significant resistivity; the conductor model implied though isotropic is, still, spatially varying and it has a large value in the scaled equivalent of the equatorial region.

Table 5. Parallel distance scaling factor and effective coupling distances from 160 km altitude.

Altitude	Local Root Conductivity Ratio $\sqrt{\sigma_{\parallel}/\sigma_{\perp}}$	Effective Z from 160 (km)
120	10	1.1
145	50	.2
160	100	0
180	200	.13
200	400	.2
220	800	.23
280	1600	.28
350	5000	.30
Conjugate F-region (estimate)		.4

In light of the effective distance values given in Table 5, it is possible to make inferences about the effect of the current bled-off by Pedersen conductivity. The table implies that the region below 120 kilometers lies in the far-field of structure produced potential variations smaller than 1 kilometer. Thus E-region conductivity probably does not play a role in the dynamics of most barium cloud structures. (This effect only makes the M-ratio discrepancy worse by effectively lowering the background conductivity to 2.9 mho for cloud structures.)

A similar comment applies to structures smaller than 400 meters and coupling to the conjugate ionosphere. Structure smaller than 400 meters would not be expected to significantly couple to enhanced conductivity in the conjugate F-region because of the bleed-off of current. The issue of whether sizes larger than 400 meters couple depends upon the conductivity of the intervening region as discussed earlier in this section.

It seems clear from the considerations of field line resistance and the considerations of Table 5 that the dynamics of the large scale JAN plasma cloud, which is of order 5 km across, should be influenced by conjugate conductivity. Conceivably it could even provide the necessary 10 mhos needed to bring the M-ratio data into agreement.

2.6 CONJUGATE COUPLING AS A SIZE SELECTION MECHANISM

The previous section noted that coupling to regions of enhanced conductivity is a size dependent phenomenon. In this section that point is emphasized to suggest that it provides a size selection mechanism which is in agreement with both qualitative and quantitative aspects of the data.

The previous section noted that larger size structures are capable of coupling to regions of enhanced conductivity

in the E-region and conjugate F-region whereas smaller structures could not. The potential fields of the larger size structures are, consequently, shorted out and, thus, they tend to resist movement with the wind more than the smaller size structures. The smaller structures within the large scale cloud tend to move out and create gradient drift structures. A breakpoint in structure behavior consequently exists at the largest structure size which does not couple to enhanced plasma conductivity. Structures this size and smaller would be expected to result from the gradient drift break-up of the cloud and they would be stable to further bifurcation.

The qualitative aspects of the mechanism are in agreement with observations of the structure size data made by Linson and Baxter (1977). They note that in a similar barium ion cloud, namely SPRUCE, structure sizes immediately after cloud bifurcation ranged from 100 to larger than 500 meters. They also note that 500 meter structures remained stable to further bifurcation suggesting qualitative agreement. Quantitative agreement is also suggested between the noted 500 meter size and the effective far-field distance to the conjugate.

Note that this sieve-like coupling mechanism of size selection can operate in conjunction with other size selection mechanisms such as diffusion and viscosity. The latter two may produce other break points in the spectrum of structure scale sizes at smaller sizes. The qualitative and quantitative appeal of the sieving mechanisms suggests that further investigation into its features is warranted.

SECTION 3

JAN STRUCTURE SIZE

The nominal size of structures generated by the JAN ion cloud is discussed in this section. There are three sources of this data, namely, photographic, aircraft, and electron density probe. Each has its own interpretational problems, nevertheless they all tend to give consistent estimates for structure sizes. Table 6 summarizes the estimates from each data source. Some sources of data specify an outer scale directly whereas others specify structure diameter. The conversion factor between the two ranges from .3535 for top hat structures (Kilb, 1984b) to $1/\pi$ for sinusoidal structures. With either conversion factor there is general agreement between the values in both columns. The following sections discuss each of the size estimates in greater detail.

3.1 STRUCTURE SIZE FROM PHOTOGRAPHIC MEASUREMENTS

Three transparent prints of color photographs of the JAN barium cloud were provided by Wallace Boquist of Technology International Corporation. The photographs were taken from a site, A-105, which provided up-the-field line views of many of the structures. By manually measuring the structure dimension on the transparency and comparing to Az-Eℓ template dimensions, (as generated in Prettie, 1982), structure size estimates can be obtained. The principal difficulty in this process is that on the film the structure dimensions are very small and difficult to measure. The nominal structure diameter from the 2343:44 (Release + 30 min.) photograph has been measured to be 240 ± 80 meters. On the photograph this size corresponds to .17 inches or less than half a millimeter emphasizing the measurement difficulty.

Table 6. JAN structure sizes.

Source	Estimated Size Outer Scale	Diameter
Optics 2343:44		
Typical Structure Size	-	240 ± 80
JAN Pass 4 Aircraft data at 2333		
Phase Perturbations FW HM	-	160 - 400
P.s.d. Breakpoint	90*	-
Rocket Data		
Apparent Fluctuation Wavelength	60 - 72	-

* favored estimate

There are many structures in the 2343:44 photograph and most seem to have roughly the same 240m size. One interesting feature is a larger parent structure in the process of bifurcating into two structures. In this feature each new structure appears to have a roughly 240 meter size, and the two are separated by a roughly 240 meter low density region apparently moving into the parent structure. This feature demonstrates that in the JAN ion cloud 720m sized structures are unstable to bifurcation. Apparently the 240 meter sized structures are stable because they are numerous and no smaller structures are apparent on the film. Thus the U-shaped structure size parameter is bracketed by the 240 meter and 720 meter diameter values.

With respect to the existence of smaller structures there are other problems with photographic interpretation--in addition to the measurement precision problem--that include image blurring through motion, improper aspect, and film emulsion effects. Images may also be hidden by ion cloud shadowing as some appear to be in the 2343:44 picture. It is difficult to assert from photographic data that structures with diameters smaller than 200 meters don't exist. Nevertheless the presence of many resolvable (but barely so) 240 meter sized structures argues for a 240 meter structure size choice.

3.2 STRUCTURE SIZE FROM AIRCRAFT DATA

Aircraft data is available from the ESL measurements of satellite fading during JAN (Marshall et al., 1982). Back propagated phase measurements from JAN pass 4 at 2333 have been successfuly obtained and are shown in Figure 9. The phase perturbations observed are fairly weak leading to the indication that only the highest and northernmost structures

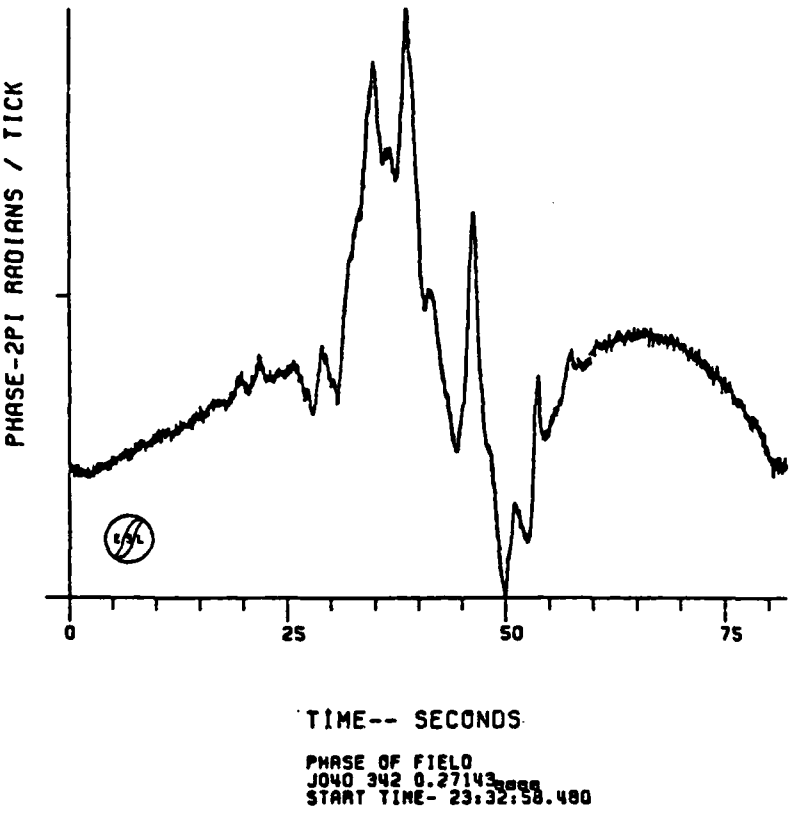

JAN Pass 4 Downlink Back-Propagated Amplitude and Phase

Figure 9. Phase of back propagated signal received at the aircraft during JAN. (From Marshall et al., 1982.)

were observed in this pass. This deficiency probably contributed to the success of the back propagation and should not overly limit the determination of structure size.

The abscissa of Figure 9 is in units of time which can be converted to distance if the aircraft speed is known. Using the distance to the S_4 minimum of 342 kilometers and the known slant range to the cloud of about 240 kilometers the nominal aircraft speed of 200 meters per second may be improved yielding a value of 240 meters per second. This value may then be used to convert all time units to distance units.

Most of the observed small scale structure sizes in the observed phase data have full-width-at-half-maximum (FWHM) durations of less than 2 seconds and greater than 1 second. One feature located at origin plus 54 seconds has a rougly 2/3 second FWHM duration. This range of values implies structure sizes of typically less than 400 meters and greater than 240 meters with one exceptional value of 160 meters.

Figure 10 shows the power spectral density of the phase fluctuations shown in Figure 9. A definitive breakpoint can be seen in the data at a frequency of .425 Hz ± .01. This frequency corresponds to a break wavelength of 565 meters and an outer scale L_o $(=\lambda/2\pi)$ of 90 meters. The size of structure responsible for this breakpoint may be loosely estimated as a half wavelength or 280 meters. This value is nicely in line with the structure size estimates from the phase data in Figure 9.

Of the many sources of data the aircraft data probably provides the most reliable structure size estimates. This fact is true in spite of the problems associated with improper aircraft positioning (as in pass 4), distortions associated with back propagation processing, uncertainties in ray path speeds through the structure and vagaries associated with structure projections.

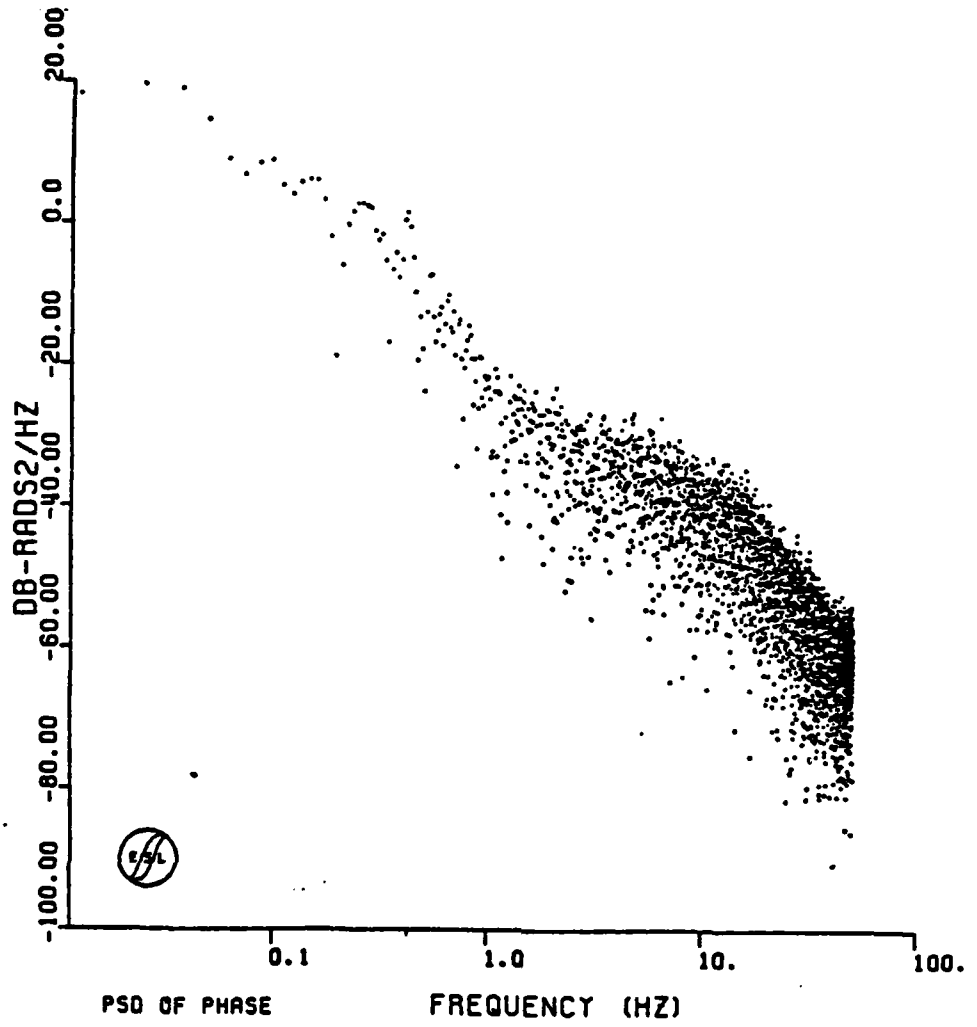

JAN Pass 4 Downlink Back-Propagated Phase PSD

Figure 10. Power spectral density of phase fluctuations seen in Figure 9. (From Marshall et al., 1982.) Values beyond 1.5 Hz are artifact.

In light of the fact that the U-shaped curve size selection model will be used to determine outer scales it is appropriate to use the 90 meter outer scale value obtained from Figure 10 as the representative aircraft value. This value is in good agreement with the values obtained from photographs as discussed in the previous section and is not out of line with rocket data discussed in the following section.

3.3 STRUCTURE SIZE FROM ROCKET MEASUREMENTS

Structure size data is available from the rocket payload measurements. Both the results of the electron density probe measurement (Szuszczewicz et al., 1981) seen in Figure 11 and the mass spectrometer measurement (Narcisi et al., 1981) show identical plasma density structures. In this section the size of these structures is estimated.

The density probe results of Figure 11 show structures that have a wavelength of roughly 1.5-1.8 seconds. While peaks and valleys are apparent with durations less than .75 seconds, they are accompanied by correspondingly longer valleys or peaks. The structure, thus, seems to be described by a fairly uniform wavelength.

The rocket speed across the striations is required to convert time scale to a distance scale. Establishing a good estimate for this speed is the primary interpretational problem with this source of structure size data. It is known that the rocket traversed the cloud from the northern side of the cloud toward the southern side as it moved upward in altitude. It is also known that the up-the-field component of the rocket motion is significantly larger than the cross-cloud motion. Quantitative values for this motion have not been published yet although they may be available from photographic records made by T.I.C. For the purposes of this report a crude guess for this speed can be made by assuming

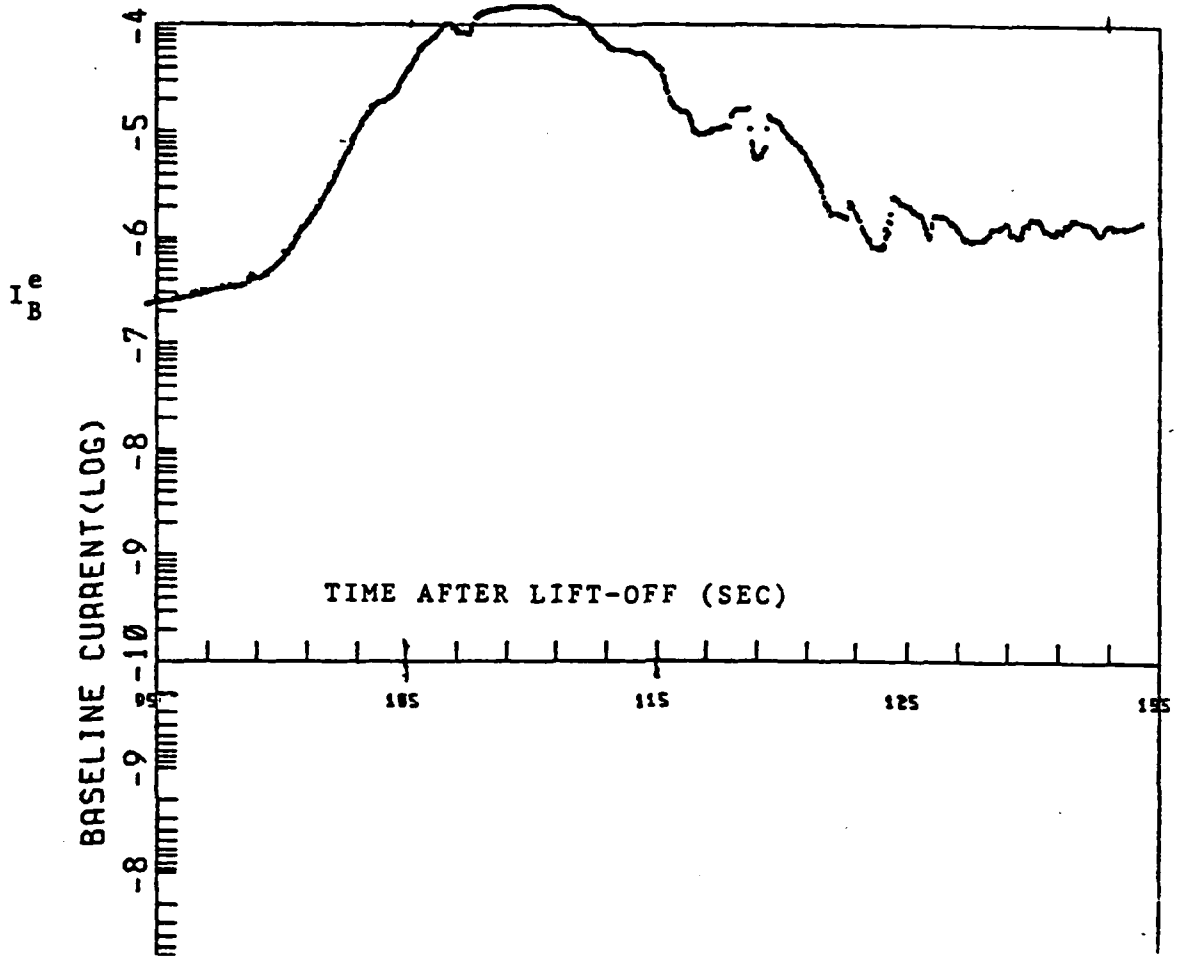

FIGURE 4 **AN EXPANDED VIEW OF THE BARIUM ION CLOUD DENSITY PROFILE AS MEASURED BY BASELINE ELECTRON CURRENTS. Absolute electron densities can be estimated within an accuracy of ± 32% (detailed analyses will yield ± 10% or better) by the conversion N_e [cm^{-3}] = 5.62 (10^{10}) I_B^e [amps].**

Figure 11. Electron density measured by JAN rocket payload. (From Szuszczewicz et al., 1981.)

that the bulk of the ion cloud has a 5 kilometer width as observed optically. From the data in Figure 11 the rocket is seen to cross this width in 20 seconds. The component of the rocket velocity transverse to the striations is consequently found to be 250 meters per second. Similar values have been obtained for the rocket trajectory across ESTHER during STRESS (Linson and Baxter, 1978).

Under a 250 meter per second rocket velocity assumption the structure wavelength of 1.5 to 1.8 seconds converts to 375 to 450 meters. Structure outer scales ($\lambda/2\pi$) are consequently found to be 60 - 72 meters. Structure sizes may be estimated as a half wavelength or 190 - 220 meters. These values are somewhat smaller than those implied by photographic and aircraft measurements, but are not so small as to be considered to be in serious disagreement.

SECTION 4

DIFFUSION CONSIDERATIONS

In this section attention is focussed on obtaining an estimate for the diffusion coefficient, D, in the U-shaped curve relation (Equation (1) appearing in Section 1). The steep gradient fronts observed in the JAN rocket data serve as the primary experimental source for this estimate. In Section 4.1 the steep gradients observed in JAN are presented and compared with similar data from the ESTHER release during STRESS. In Section 4.2 an analysis is made of the gradients to determine a value for the diffusion constant.

4.1 COMPARISON OF GRADIENT LENGTHS MEASURED IN JAN AND ESTHER

Section 3.3 discussed the electron density data available from the electron density probe measurements (Szuszczewicz et al., 1981) made during JAN. In Figure 11 the density data measurement across the entire cloud is presented. Data with higher resolution is also available and, though its quality is marginal, inferences may be made about the gradient lengths of the steepened structures in JAN. In this section these lengths are evaluated and compared with similar measurements made during the STRESS event ESTHER.

The density probe flown through JAN sampled the plasma density at a 4 kilo sample per second rate. Portions of the data resolved on a sample by sample basis are available for this report. The data is of marginal quality, however because the portions are available only once a second and have only a quarter second duration.

Figure 12 shows an example of the high resolution data that is available. It shows a steep gradient front which

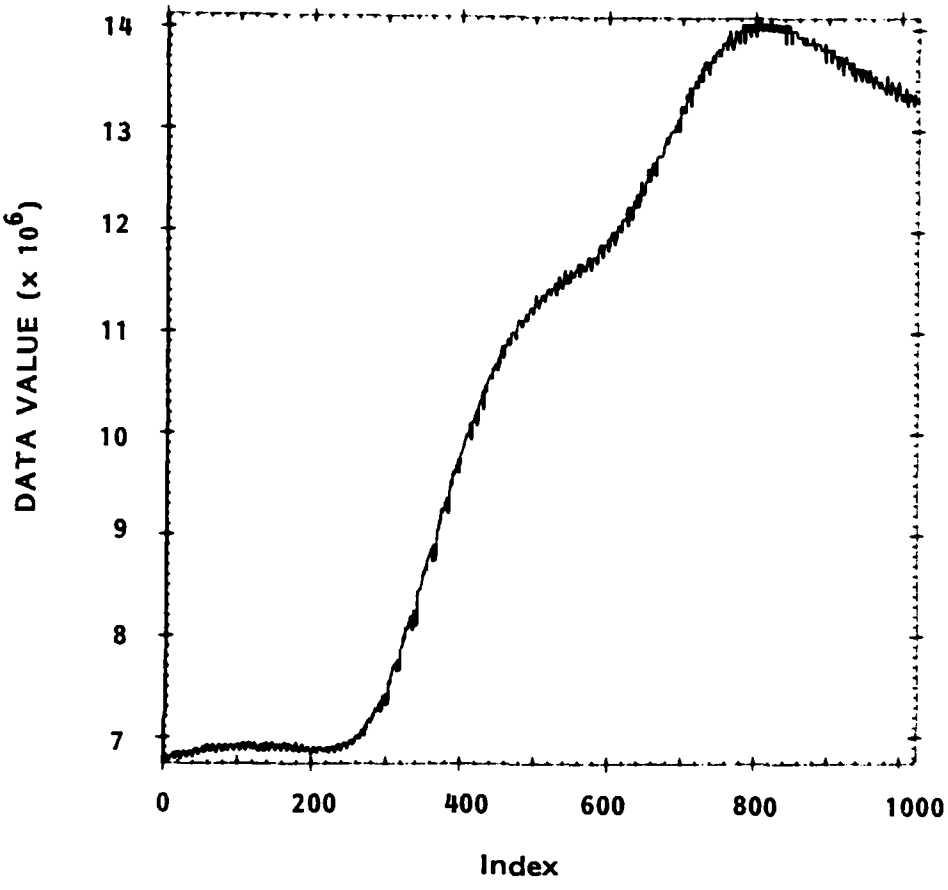

Figure 12. Steep density gradient observed in JAN. The abscissa units are samples (1/4 msec). The ordinate is directly proportional to density. (Plot obtained from raw data provided by Szuszczewicz.)

is fortuitously captured in the quarter second plot near 2344:50. In this plot a factor of 2 change in density occurs in one-eighth of a second or, assuming the 250 meter second rocket speed suggested in Section 3.3 in a distance of 32 meters. Perhaps more surprising is that this feature seems to consist of two features one with a still steeper gradient. At the steeper gradient the density appears to change at the rate of e-folding every 25 meters.

Steep edges were also observed by the Utah State probe flown through the STRESS cloud ESTHER as seen in Figures 13 and 14 from Kilb (1984). If one assumes an 800 meter per second velocity (as does Kilb, 1984) the edge dimension corresponds to e-folding in density every 16 meters in Figure 13 and to e-folding every 8 meters in Figure 14.

Table 7 summarizes this comparison between ESTHER and JAN gradient lengths. The difference in the values is surprising especially in light of the higher ion-neutral slip speed believed to be appropriate for JAN (50 m/s vice 32 m/s estimated for *ESTHER (Linson and Baxter, 1978)*). The differences in values could arise from any combination of the following factors:

1. JAN structures are traversed where the ion neutral slip speed is locally small (wind shear?) or where the structures are poorly developed (near the leading edge?).

2. ESTHER striations are steeper because they are older (48 1/2 minutes vice 30 minutes for JAN).

3. The assumed rocket velocity for JAN of 250 meters per second is significantly in error (by as much as a factor of 2 too large) which implies that the measured structure sizes of Section 3.3 are still smaller than estimated therein.

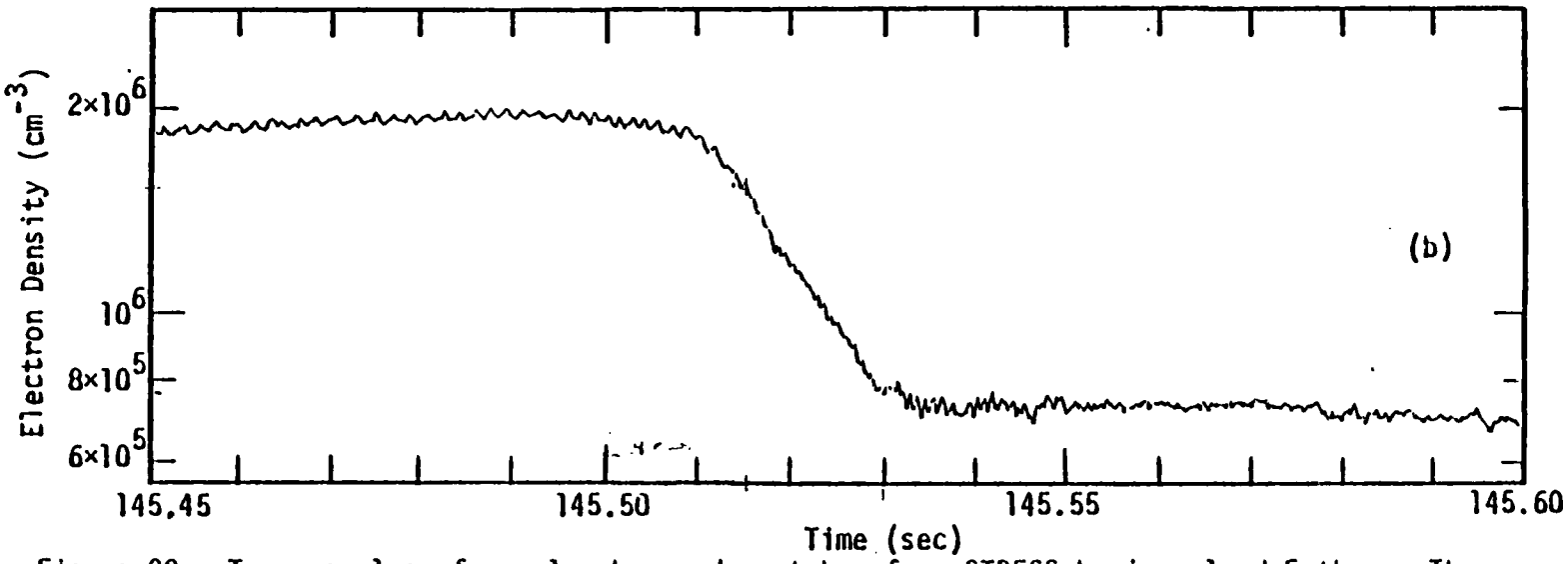

Figure 22. Two examples of nearly sharp edges taken from STRESS barium cloud Esther. There are 100 data points between tic marks. To convert time to distance, use $x = v_{\perp}t = 800\ t$ meters.

Figure 13. Steep gradient observed by ESTHER rocket probe. (From Kilb, 1984.)

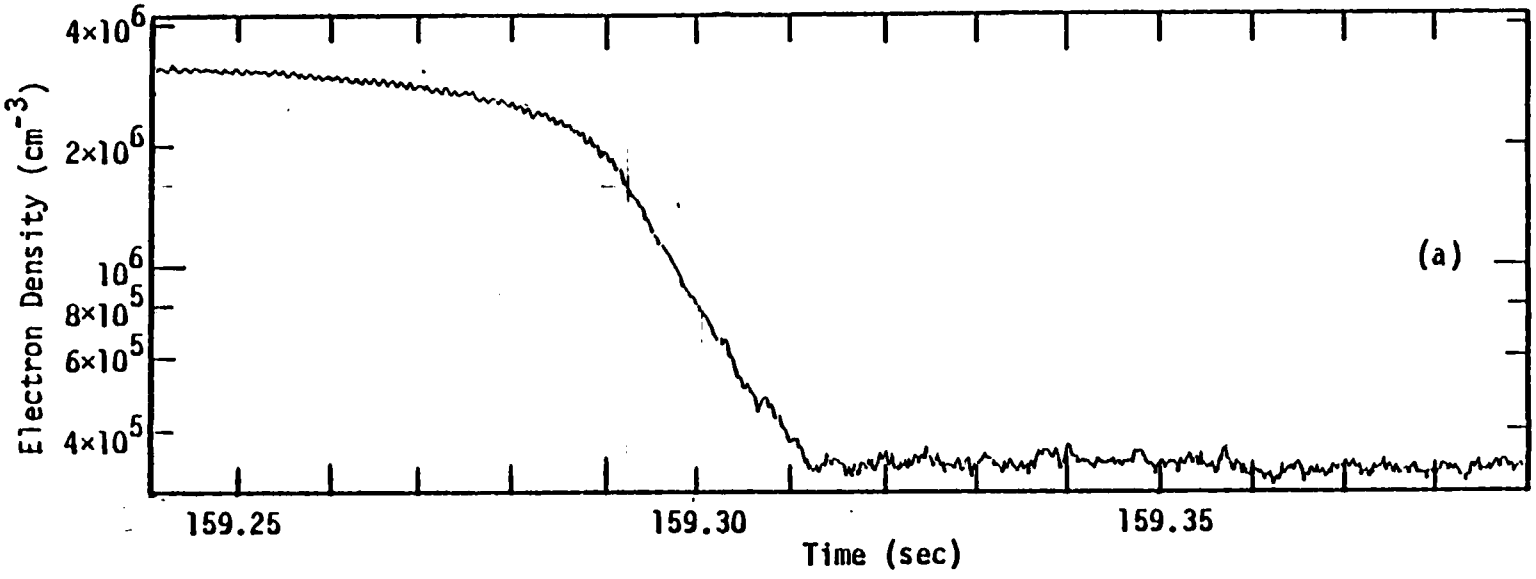

Figure 14. Another steep gradient from the ESTHER rocket probe. (From Kilb, 1984.)

Table 7. Comparison of gradient lengths in JAN and ESTHER.

Feature	(meters per neper)	Assumed Speed (m/s)
ESTHER		
145.52	16	800
159.3	8	800
JAN 2345:50		
Average slope	45	250
Steepest	25	250

4.2 ANALYSIS OF DENSITY GRADIENTS TO ESTIMATE THE DIFFUSION PARAMETER

The effective diffusion constant plays an important role in the U-shaped curve size selection relationship (Eq. 1). Various cross-field diffusion mechanisms have been suggested, and the range of diffusion constants that they predict covers two orders of magnitude. An attempt to narrow this range certainly seems to be warranted in order to reduce the uncertainty in the U-shaped curve parameter, R, which results from this report. One experimental source for the value of the diffusion constant is the rocket probe measurements of steep density gradients. Diffusion plays a strong role in the establishment of these steep gradients and their shape can reveal insights into the quantitative nature of the diffusion process. In this section, an analysis of the density gradients measured by the density probe flown through JAN is presented.

Three processes could be responsible for plasma cross-field diffusion, namely:

1) electron-neutral collisions

2) electron-ion collisions

3) enhanced electron diffusion due to coupling

The values for the diffusion constant from each mechanism and their dependence upon plasma density are tabulated in Table 8 and they are seen to range from 1.5 - 15 meters squared per second. By comparison the unimpeded ion diffusion rate is 150 m^2/s. (This value has also been suggested for use in the U-shaped curve relation.)

From the Table it is seen that for nominal barium cloud parameters the diffusion process is predicted to be dominated by coupling effects. The coupling diffusion mechanism is

Table 8. Diffusion values.

Mechanism and Conditions	Diffusion Constant (D_o)	Dependence on Plasma Density	Diffusion Drivers $\left(D\frac{n_{xx}}{n_x} + D_x\right) \Big/ D_p$*
Electron-neutral collisions @ 160 km altitude	1.5 m^2/s	Independent	$\frac{n_{xx}}{n_x}$
Electron-ion collision @ (3×10^6 el/cc)	1.5 m^2/s	Directly Proportional	$\frac{nn_{xx}}{n_p n_x} + \frac{n_x}{n_p}$
Coupling-- Conductivity Ratio + 1 = 10 Altitude = 160 km	15 m^2/s	Inversely Proportional	$\frac{n_p n_{xx}}{nn_x} + \frac{n_x n_p}{n^2}$

* D_p is the diffusion constant appropriate for plasma with density n_p. The 'x' subscripts denote differentiation.

effective provided that the electrostatic field of a structure can couple to a background region which has a spatially uniform integrated Pedersen conductivity. In developing the estimate in Table 8 it is assumed that this background has 10% of the structure's peak conductivity. The creation of images and plasma resistivity in the direction along the field lines may limit the coupling process. If this process is limited sufficiently, then diffusion of regions with densities greater than 3×10^6 electrons per cc would be predicted to be dominated by electron-ion collision effects and lower densities would be dominated by electron-neutral effects.

The classical explanation for the steep edges found in barium cloud density profiles is that they are the result of the higher density portions of the barium cloud tending to move faster than the lower density regions. Except for diffusion effects the flow of the plasma would be incompressible, and infinitely steep gradients would be produced. Diffusion limits the gradient size because its component of flow increases with increases in the magnitude of the density gradient. An equilibrium state can consequently be defined as the balance between the steepening and diffusive influences.

If certain assumptions are made regarding the balance between steepening and diffusion then the rocket probe measurements of the steep density profiles may be used to determine diffusion coefficients. These assumptions are as follows:

1) The feature measured represents a feature that is an equilibrium between wind driven steepening and diffusion.

2) The electrostatic field in the feature may be approximated as that which would result in the wind driven edge of a radially symmetric cloud with the same profile.

The first assumption is required in order to even approach the problem. If it is a poor approximation because the edge has not fully steepened, then the estimated diffusion constant values will be too large. The second assumption is required in order to get a grip on the steepening rate of the wind driven flow. Its assumption is equivalent to assuming a rocket trajectory through a feature similar to that shown sketched in Figure 15a. If the trajectory is somewhat off angle from the wind driven axis and is more like that shown in Figure 15b, then the estimated diffusion constant values will be larger than actual, but only by small factors according to the secant of the off-angle.

An equilibrium of steepened contours implies that all contours move with a constant speed. The speed of a density contour along the axis of the wind, x, is given by n_t/n_x (where n is the density and subscripts denote partial differentiation), and, consequently,

$$\frac{n_t}{n_x} = \text{constant} \qquad (10)$$

provides a starting point for the analysis. The continuity equation along this axis is to a good approximation given by

$$n_t = \phi_y \, n_x + \left(Dn_x\right)_x \quad (@ \quad y = 0) \qquad (11)$$

where ϕ is the electrostatic potential, D is the diffusion constant and where the small contribution of $\left(Dn_y\right)_y$ has been neglected. Equation (11) may be substituted into equation (10) to give the cornerstone relationship

$$\phi_y = D \frac{n_{xx}}{n_x} + D_x = \text{constant} \qquad (12)$$

Using assumption 2) the value of ϕ_y may be estimated. Once both ϕ_y and an estimate for the spatial dependence of the plasma density n have been determined, the diffusion constant may be estimated.

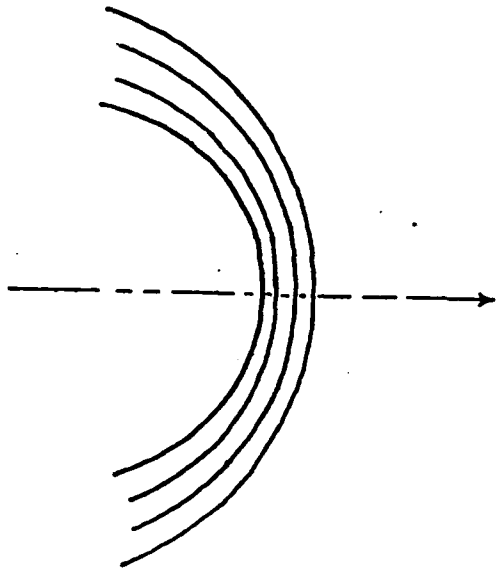

Figure 15a. Assumed rocket trajectory through density contours.

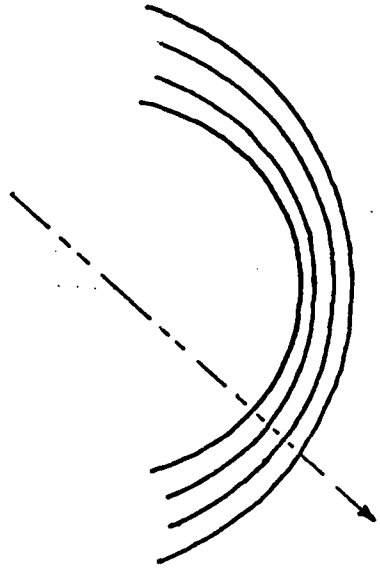

Figure 15b. Off-axis trajectory through density contours. The density gradient measured is somewhat less than in Figure 15a.

The evaluation of ϕ_y is now considered in greater depth.

Using the second assumption the potential function, ϕ, may be evaluated in terms of the measured density profile. The potential equation

$$\nabla \cdot (n \nabla \phi) = - V n_y \tag{13}$$

where V is the wind speed may be transformed with the assumption that n is radially symmetric. Under this assumption the potential $\phi(x,y)$ is separable in circular coordinates r, θ and may be written as

$$\phi(x,y) = \phi(r) \sin(\theta) \tag{14}$$

giving

$$\phi_{rr} + \left[\frac{1}{r} + A(r)\right] \phi_r - \frac{\phi}{r^2} = - A(r) V \tag{15}$$

where $A(r) = (\ln n(r))_r$.
Equation (15) is a second order differential equation which depends on the local density through the function $A(r)$. The function $A(r)$ is zero whenever the density is constant and in these cases the solution reverts to its homogeneous solutions, r or $1/r$. Over the region in which the density has a non-zero gradient and $A(r)$ is non-zero, the potential is most easily solved for numerically.

The important quantity for the cornerstone relation (12) is not the potential ϕ but is instead its y-derivative, ϕ_y. Once ϕ has been determined the value of ϕ_y is given by

$$\phi_y = \frac{\phi}{r} \tag{16}$$

Note that ϕ is typically a smooth function even near steep gradients and consequently ϕ_y is expected to be smooth.

The data from the JAN rocket probe near 2344:50 as shown in Figure 12 has been digitized and used to estimate the values of ϕ_y. The density profile appears to consist of two steepened diffusing features, one at higher density and one at lower density. The digitization started near the inflection point between these two features and then proceeded in such a manner to include only the lower density feature. The radius of the cloud at the first point in the digitized data has been assumed to correspond to a 150 meter radius in line with the approximate breadth of this structure. The rocket velocity through the structure has been assuemed to be 250 meters per second, per the discussion in Section 3.3.

The Runge-Kutta method sketched in item 25.5.20 of Abramowitz and Stegun (1970) has been used to find both homogeneous and particular solutions across the density gradient. The solutions have been combined to match a pure r-like interior dependence and a pure 1/r-like exterior dependence in the potential equation. The wind speed has been chosen such that the interior ion-neutral slip speed is 17 meters per second. This is an important assumption because it is related to the assumed M-ratio as discussed in Section 5.

The value of ϕ_y which results from the calculation for JAN, is shown in Figure 16. This value is also the negative of the x-component of the plasma velocity. Over the 26 meter interval of the calculation the x-directed velocity slows by nearly 5 meters per second and its magnitude is such that the expected steepening is produced. Figure 16 represents the evaluation of the first term of the cornerstone equation, eq. (12). Evaluation of the second and third terms from the data up to a diffusion related coefficient is also possible.

Table 8 lists in the final column, the dependence of the diffusion terms on the measured density. By evaluating

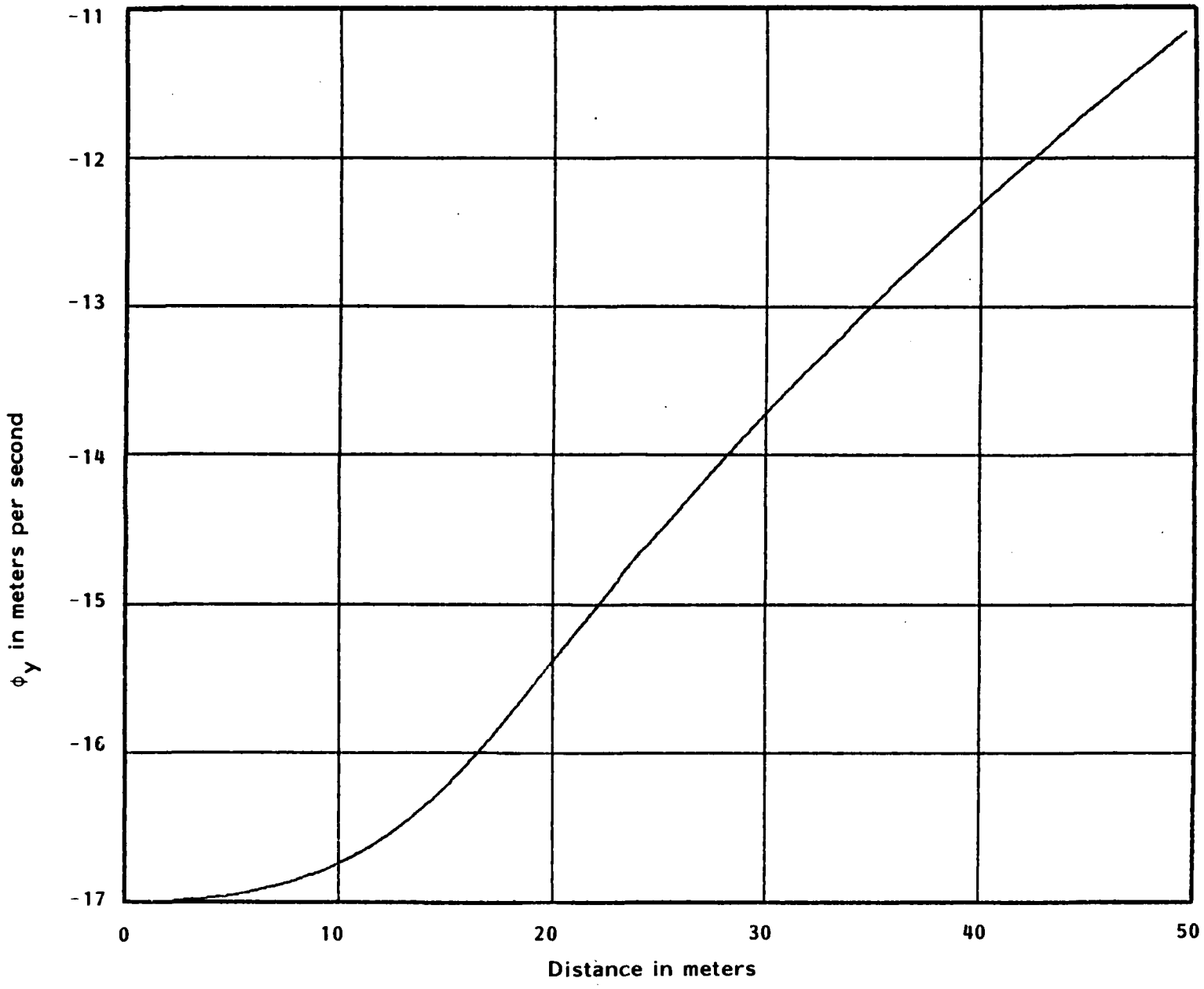

Figure 16. The y-derivative of the potential. The negative x-component of plasma velocity.

the density related terms agreement between the theoretical dependence given by equation (12) and the data can be investigated. The diffusion constant can also be found.

Figures 17 through 19 show plots of the distance dependence of the following:

1) The density values used aft r hand digitization and smoothing. (Figure 17)

2) The first and second derivatives of density. (Figure 18)

3) The diffusion drivers listed in Table 8. (Figure 19)

The lack of digital data necessitated hand-digitization. For evaluating second derivatives smoothing is very important.

In Figure 19 it is seen that the curves are all similar reflecting the fact that n_{xx}/n_x is the most important contributor to the diffusion driver terms. The electron-neutral dependence lies generally between that of the electron-ion and coupling driven curves as would be intuitively expected. All the curves pass through zero near the middle of the structure gradient providing a point at which the arbitrary constant of equation (12) may be straightforwardly evaluated. The erratic behavior of the curves near 22.5 meters is due to the first derivative of the smoothed data, in going slightly positive, passes through zero making n_{xx}/n_x indeterminate. The positive value for the final derivative is an artifact of the smoothing routine.

With the constant in equation (12) determined it is possible to solve for the diffusion constant on a point-wise basis. The result is shown in Figure 20. Figure 20 not only provides an estimate for the in situ diffusion constant but it also provides an indication of which diffusion

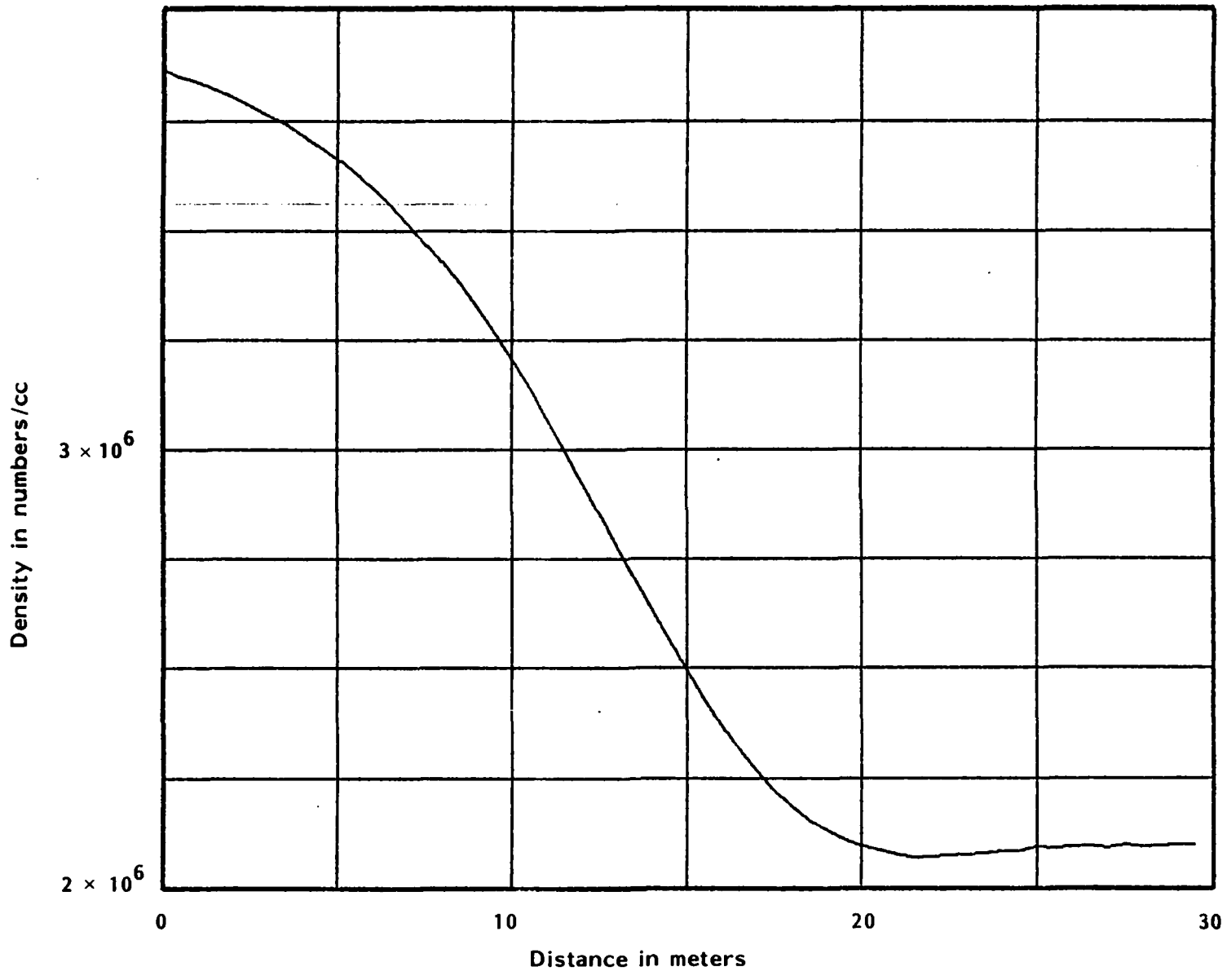

Figure 17. Density values from steep gradient in JAN measured near 2344:50 vs distance. Density has been hand digitized and smoothed.

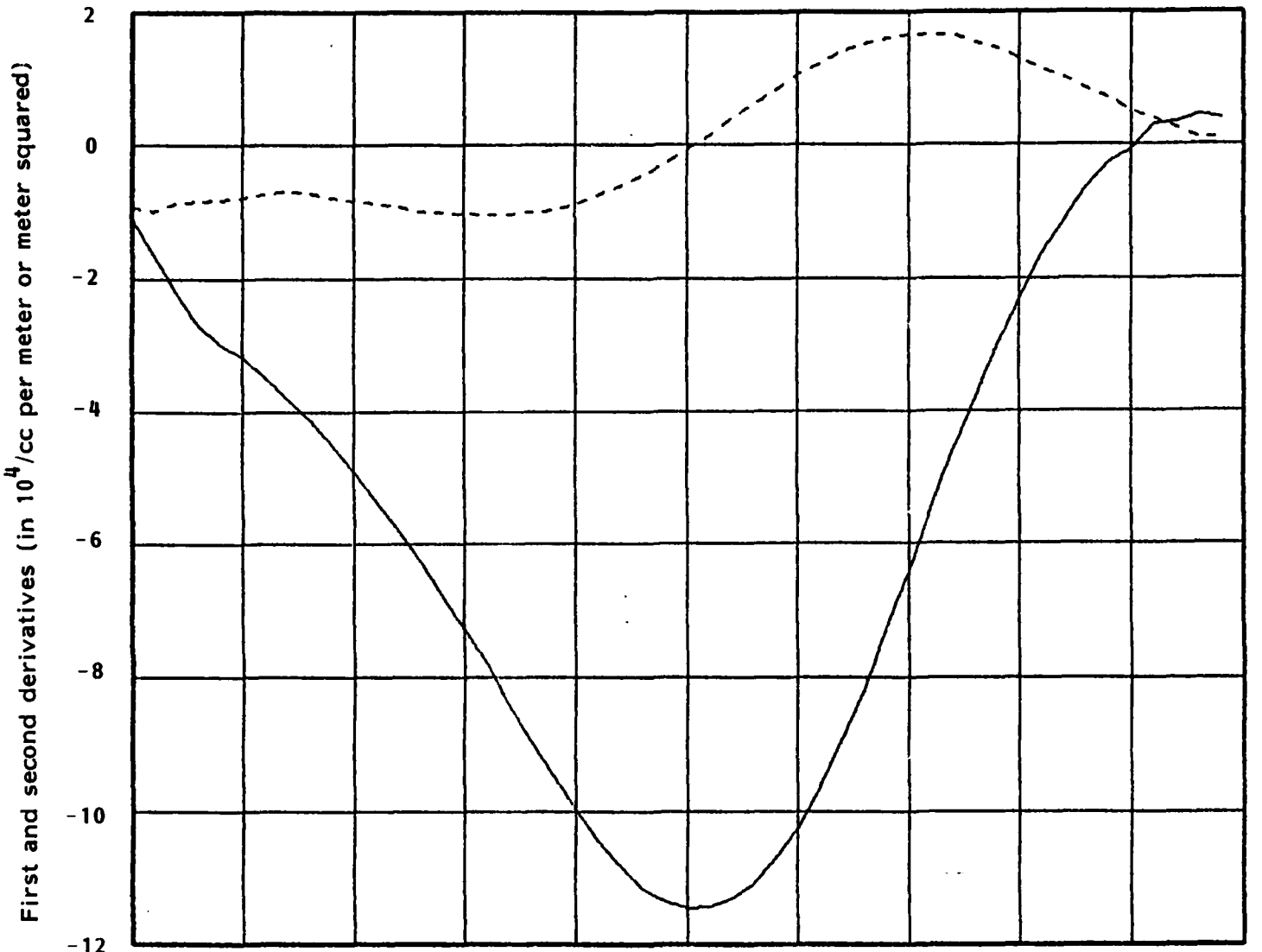

Figure 18. Values of n_x (solid) and n_{xx} (dotted) computed from data.

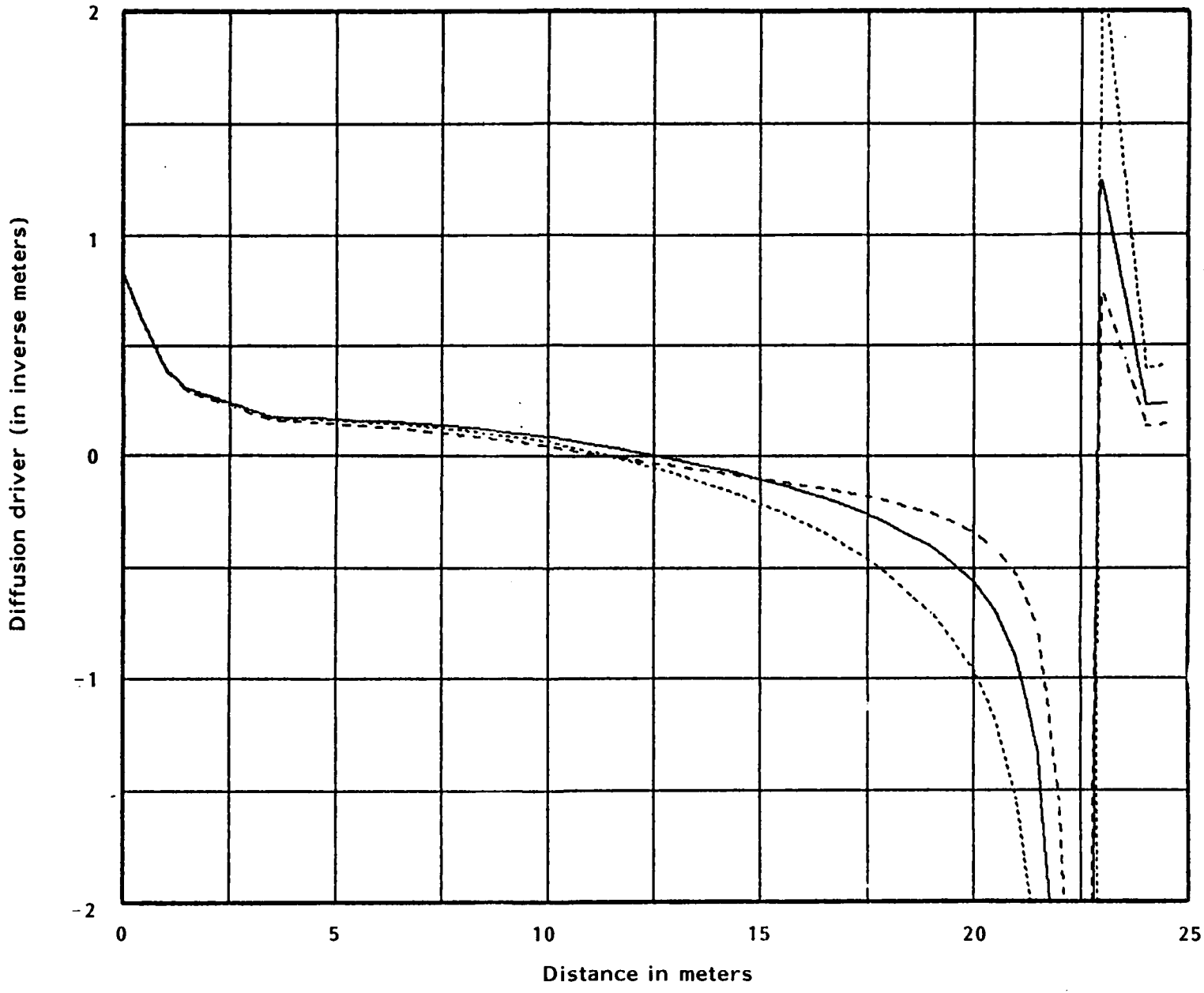

Figure 19. Values of diffusion drivers enumerated in Table 8. Electron-neutral (solid), electron-ion (longer dash), coupling (shorter dash).

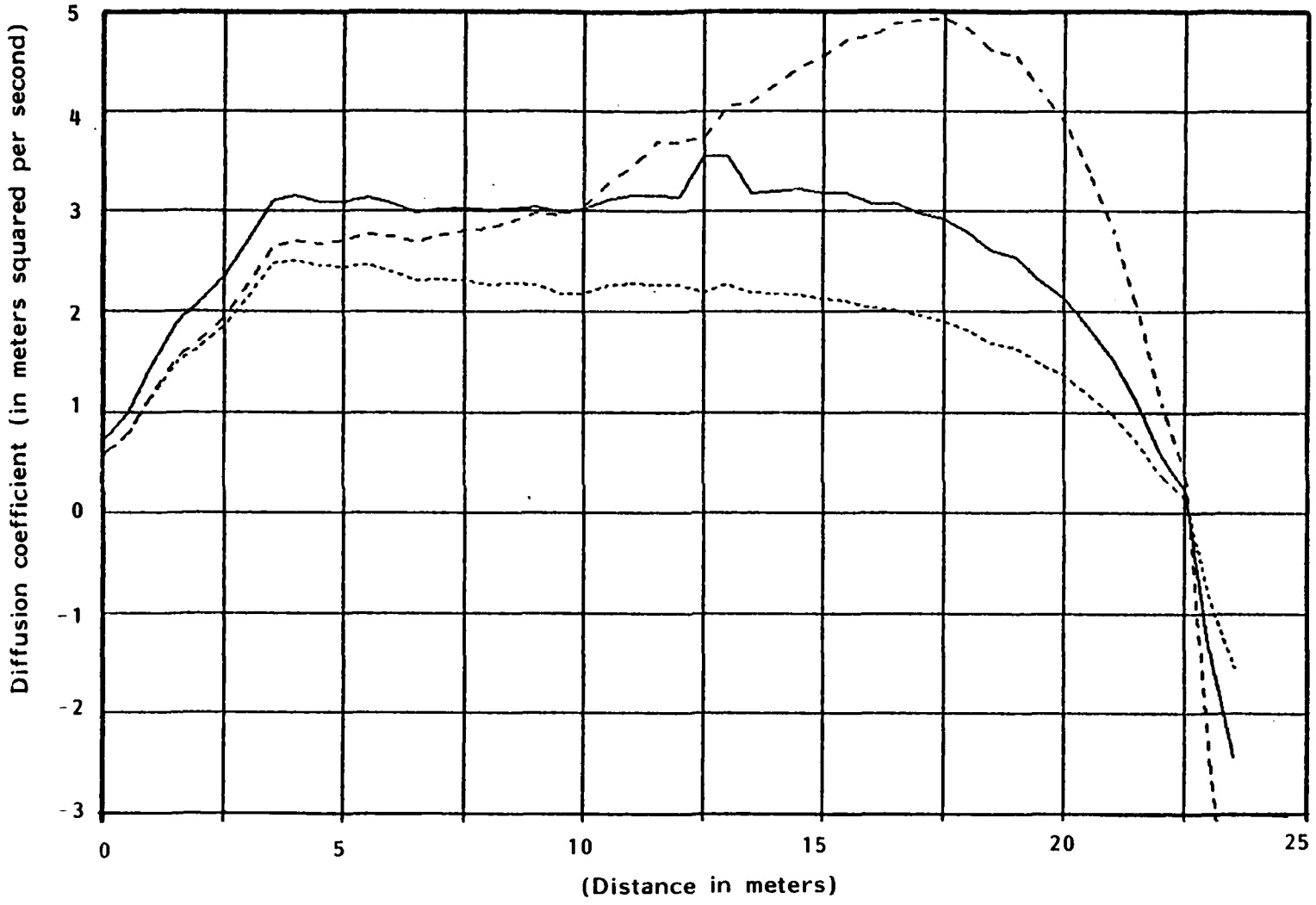

Figure 20. The diffusion constant resulting from analysis. Electron-neutral (solid), electron-ion (long dash), coupling (short dash). Electron-neutral diffusion coefficient is the one that is most nearly constant.

mechanism is operative. The degree to which the plotted data is constant reflects the accuracy of equation (12) and the assumptions leading to it since the value of the implied diffusion rate at peak density, D_p should be constant. Based upon these observations, the plots of Figure 20 seem to point to the results that electron-neutral collisions dominate the diffusion process and that the diffusion constant has a value of roughly 3 meters squared per second. These are the significant results of the diffusion analysis.

What is perhaps most surprising about the results is the absence of enhanced diffusion through coupling effects. One potential explanation for its absence is that enhanced diffusion through coupling would tend to be more pronounced near the lower density portion of the density profile and that in this region the data smoothing routine may have distorted some of the data. Nevertheless, visual inspection of the edge features of both JAN and ESTHER reveals the impression that the second derivative of the density is much smaller in magnitude near the top of the cloud than near the bottom. All of the edges appear smoother near the higher density regions. This appearance argues more for the contrasting behavior predicted for the electron-ion collision diffusion mechanism than for the behavior produced by the coupling mechanism of diffusion. The implication is that the striations, whose edges are shown in Figures 12, 13, and 14 did not couple to any noticeable background conductivity or that the regions to which they did couple had very similar conductivity profiles.

SECTION 5

RESULTS AND CONCLUSIONS

In the previous sections the parameters for the determination of the U-shaped curve proportionality ratio, R, have been determined from experimental data. Section 5.1 combines these results to estimate its value. This value is compared with results derived from numerical simulation in Section 5.2. Conclusions are then presented in Section 5.3.

5.1 U-SHAPED CURVE PARAMETER IMPLIED BY JAN DATA

In this section the results of the previous sections are reviewed and discussed to provide justification and caveats for the U-shaped curve proportionality constant results that are presented in Table 9. Table 9 presents the values of the R-ratio, that result from the data under different interpretations of the M-ratio data.

In Section 2 the best estimate of the M-ratio of the JAN structures is found to be 15. Other estimates are also given as noted in Table 9. The estimate of 15 is based on the assumption that the structures themselves do not couple well to the conjugate ionosphere and that their dynamics and correlation with the U-shaped curve should be reflective of only the local background ionosphere. The estimate is arrived at using phase data from the aircraft to determine the cloud conductivity and using rocket data to determine the background conductivity. The neutral density required for the conductivity calculation is evaluated from a standard atmospheric model. Although deviations from the neutral density model will cause significant changes in the conductivity values, the M-ratio is insensitive to these changes because cloud and background conductivity will be affected in approximately the same manner. The primary source of error in this estimate

Table 9. U-Shaped curve parameters implied by JAN data.

M	$L_k UD$	$L_d U/D$	R_k	R_d	Determination of M
3	1,000	3,100	130	390	Coupling as determined from photographs assuming highly elliptical conductivity contours
5	1,500	4,700	180	560	Coupling as determined from photograps assuming round contours
15	4,000	12,000	220*	680*	Integration of Pedersen conductivity of local ionosphere
100	25,000	79,000	240	760	Observation of lack of enhanced diffusion with assumption that lack is caused by no background to couple to

$$R = \left(\frac{LU}{D}\right)\frac{M-1}{(M+1)^2}$$

L = 90 meter break point scale length (k) or
280 meter diameter (d)

U = 50 meters per second

$D = 3\left(\frac{6}{M+1}\right)$ meters squared per second

*Favored result

is the accuracy of the rocket data. Later estimates of the rocket probe current-to-density conversion factor dictate a 30% lower background conductivity value and a correspondingly higher M-ratio.

A downward variation from the value of 15 is obtained if the optics data is used as the source of the M-ratio. A range of values is possible according to the ellipticity of the high density regions of the structure as discussed in Section 2. However, the optics data may not truly reflect the appropriate M-ratio because the cloud as a whole may couple to the conjugate ionosphere whereas the structures themselves may not. Because of the time integrated nature of the photographic M-ratio determination the structure dynamics might be biased by the lower M-ratio cloud dynamics at early times when conjugate coupling is a potentially significant influence.

In Section 3 an estimate of the structure size is made. From rocket, aircraft and photographic data the size of the structures which result from bifurcations is estimated to be roughly 280 meters. The power spectra of the cloud features in aircraft phase data is found to have an equivalent break point at an inverse wavenumber of 90 meters. Either size may be used in the determination of a U-shaped curve proportionality constant R so long as once the choice is made it is recognized that the curve derived describes the corresponding parameter. For describing sizes relevant to propagation disturbances it is probably more appropriate to use the inverse wavenumber descriptor and for comparing to previous numerical simulations the diameter is more appropriate. Both terms are used in the R evaluations shown in Table 9.

In Section 4 an estimate of the diffusion coefficient is produced from the rocket data. The measured density profiles are assumed to result from a balance between diffusion and

steepening and a diffusion constant of 3 meters squared per second is found. In the analysis the steepening rate is determined from the measured density profile, the measured ion-neutral slip speed of the background, and the assumed ion-neutral slip speed inside inside the structure that is analyzed. Implicit in the interior slip speed assumption is an assumption about the M-ratio of this structure; that is, in assuming the interior slip speed to be 17 m/s when the background slip speed is 50 m/s an M-ratio of roughly 5 has been effectively assumed in the analysis. If the M-ratio of the measured structure differs from this value then the steepening rate and consequently the derived diffusion both require modification. Because the steepening rate depends inversely upon M+1 and because the diffusion constant depends directly upon the steepening rate, the diffusion constant for arbitrary M-ratio may be estimated as the 3 meter squared per second value times the correction factor 6/(M+1), as indicated in the table notes.

Note that the above comments hint at one method to explain away the discrepancy between the derived value for D of 3 meters squared per second and the theoretically predicted value of D of 1 meter squared per second which is appropriate for the structure's 170 km altitude. If the structure measured by the rocket probe has an interior slip speed of 6 meters per second, as would be the case for M = 15, instead of the assumed 17 meter per second value then the value D = 1 meter squared per second is determined by the analysis of Section 4.2 and the discrepancy disappears.

The R values that result from the analysis vary modestly with the chosen M-ratio. In light of the comments of Section 2.6 regarding the lack of coupling of smaller scale potential variations to conjugate region conductivity enhancements, it seems appropriate to favor the M = 15 choice for R. This value for M also brings the measured and the

predicted electron-neutral diffusion coefficients in line. Thus $R_d = 680$ is the favored value. The implied result is thus, that structures with diameters such that $R_d \leq 680$ do not bifurcate and merely deform and diffuse. Structures with larger diameters tend to decrease in size through bifurcation or deformation until R_d is approximately equal to 680. This result is the fundamental conclusion of the JAN data analysis.

5.2 COMPARISON WITH NUMERICAL RESULTS

The value for R and LU/D at certain values of M can be compared with numerical studies of gradient drift structuring in barium clouds. The general result of these comparisons is that the value of R derived from the JAN data is significantly larger than that derived from numerical results.

The classic work in the numerical simulation of U-shaped curve behavior is that of McDonald et al. (1981). In this work the diffusion constant required to prevent a striation tip from structuring is found. Figure 21 shows a reproduction of one of their results for an $M = 5$ striation. The initial structure in both cases has a 1 kilometer e-folding radius and is driven by a 100 meter per second wind. In the right hand panel of Figure 21, i.e., the 200 m^2/s unstructured case, the radius of curvature of the steepened front appears to be 1 kilometer. In the left hand panel which displays results with a 100 m^2/s diffusion coefficient, the radius of curvature of structure tips appears to be roughly 500 meters. Both results thus point to a value of L_dU/D of 1,000 where L_d is defined as an equivalent diameter equal to twice the radius of curvature. The implied value for R_d (not to be confused with McDonald et al.'s (1981) 'R' which in his

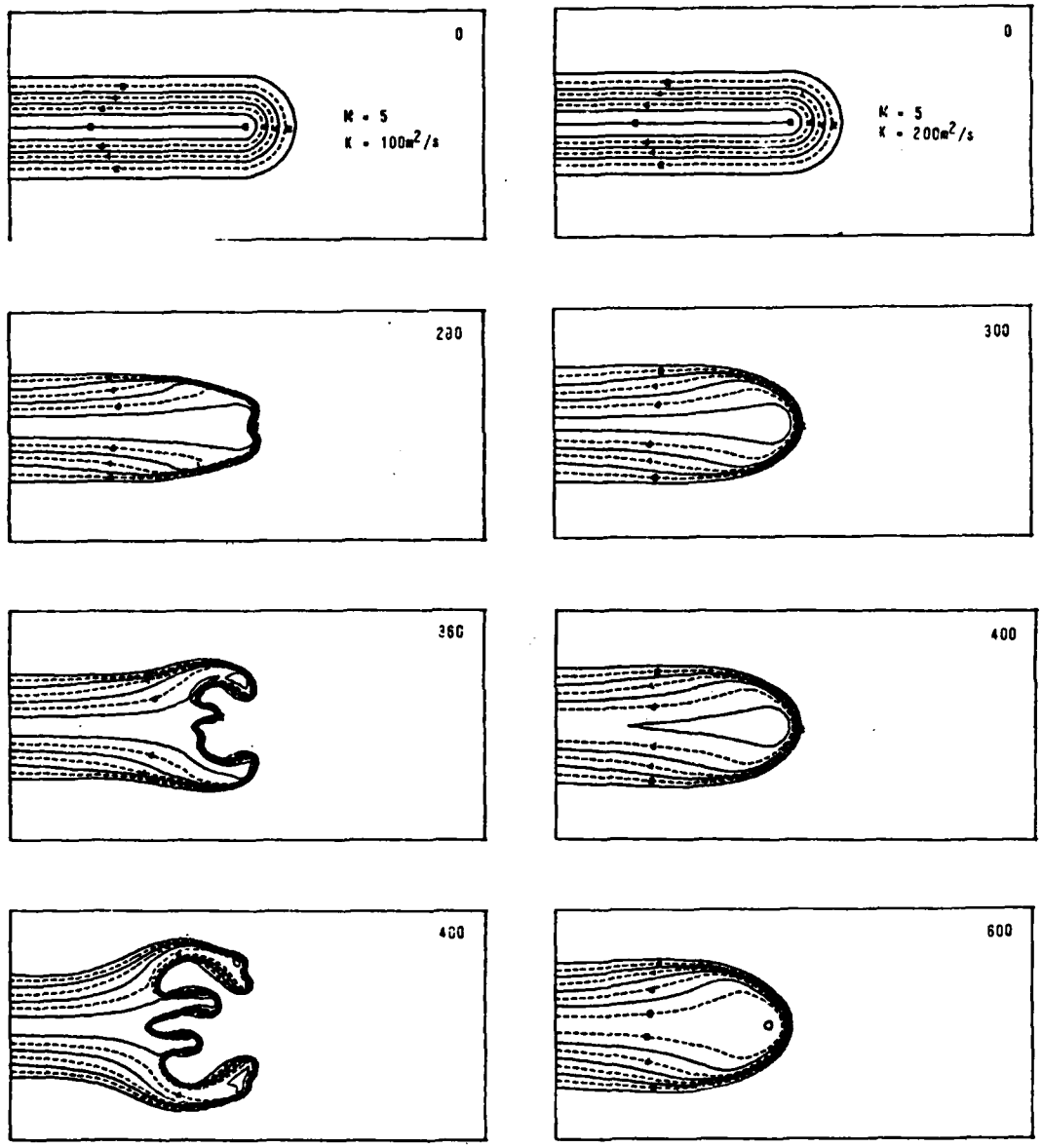

Fig. 2. Same as Figure 1 for $M = 5$. The diffusion dominated case is plotted at 300 s, the time at which L_0 attains a shallow minimum (see Figure 5). Past this time diffusive dominance is evidenced by the drying up of inner contours.

Figure 21. Numerical simulation of gradient drift structuring. (From McDonald et al. (1981).)

terminology for L_dU/D) is 110. This value is significantly lower than that implied by the JAN data.

The difficulty found in matching numerically derived barium cloud scale sizes to observed scale sizes is reflected in McDonald et al. (1981) by their appeal to Bohm diffusion as a source for enhanced diffusion. There is neither evidence for the existence of Bohm diffusion nor any theoretical indication that it should exist in barium cloud striations.

One alternative source for the discrepancy is the nature of the structuring which occurs in the results of McDonald et al. (1981). All of the structuring is of numerical origin and results from grid limitations or inaccuracy in flow potential calculations. For the structured case in Figure 21 the theoretical gradient length is of order of the cell size. A conceivable explanation for the low value of R that is obtained is that structuring is occurring artifically and at sizes dictated by the sampling mesh chosen; and thus, instability to structuring is indicated by the numerical results at sizes that in actuality might be stable.

Numerical computations with better spatial resolution have been performed since the McDonald et al. (1981) publication. These calculations show that structures initially smooth and having values of L_dU/D comparable or even a factor 3 greater than the structured case in the left-hand sice of Figure 21 do not bifurcate. There is some indication, however, that if the structures start above the U-shaped curve then they will attempt to deform toward the curve as seen in Figure 22. Figure 22 presents the results of four high resolution calculations all performed with an initial M of 4. The trajectories of L_dU/D in time are shown plotted on a U-shaped curve. The structure which started above $L_dU/D = 3000$ moved rapidly down while those two cases which started below 500 initially moved rapidly upward. The

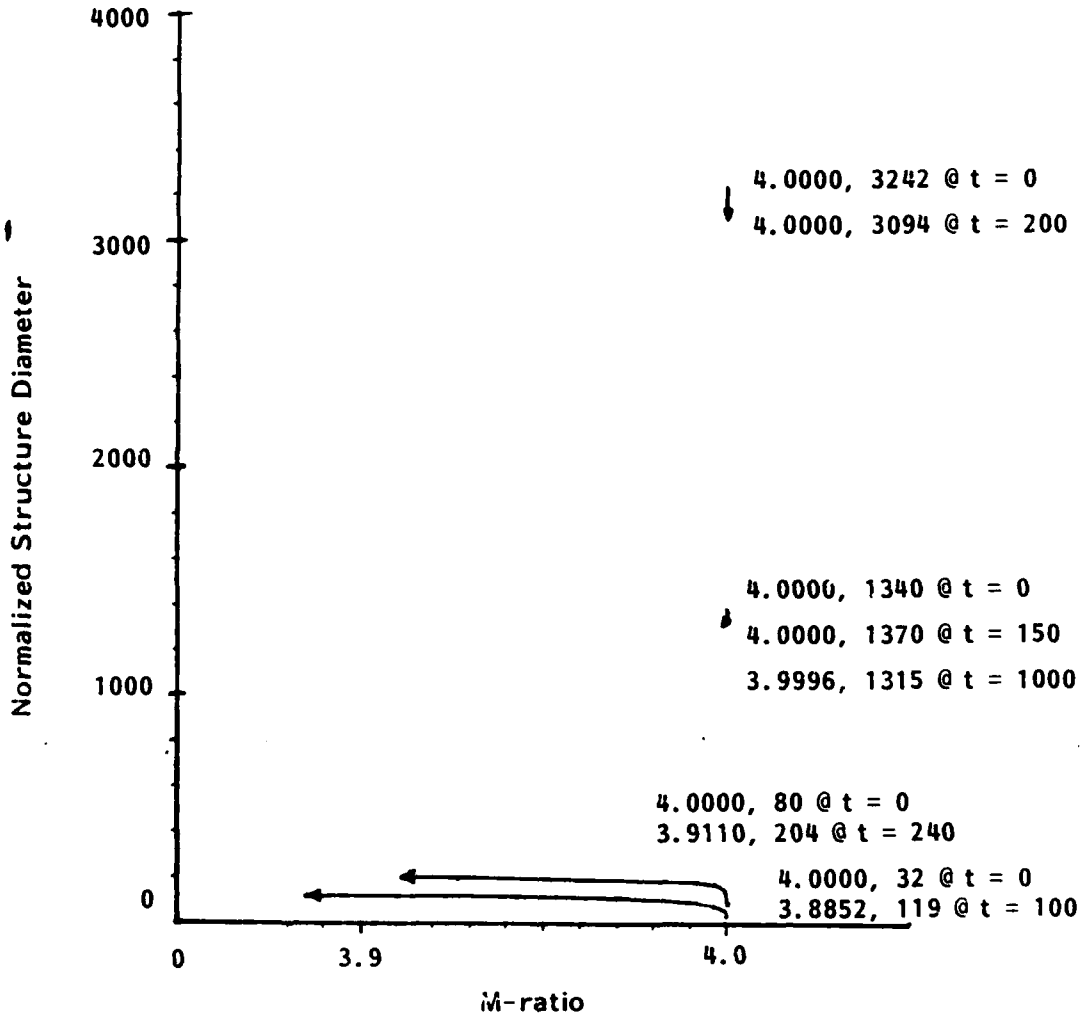

Figure 22. U-shaped curve trajectories taken by the structures in four different numerical calculations. The structure diameter is defined as the radius of the curvature of the trailing edge times 2.

structure which started near $L_d U/D = 1000$ moved first upward but, after 150 seconds, turned around and moved slowly downward. These results, though not thoroughly conclusive, hint at a possible U-shaped curve value of $\cong 1000$ and corresponding R_d value of 110 in (perhaps coincidental) agreement with the results of McDonald et al. (1981). This result is not completely conclusive because of the limited amount of data available at the larger sizes and the possible role of the varying aspect ratios of the initial structure.

Similar calculations are currently being performed with random structure seeding the cloud. The result of these calculations is that the $L_d U/D = 1000$ case will deform and possibly bifurcate. On the surface this result gives further weight to $R \gtrsim 100$ as the numerically determined U-shaped curve parameter.

In conclusion it appears that a potentially significant discrepancy exists between the value for R as determined by barium cloud data and the value determined by numerical simulations of gradient drift phenomena. This discrepancy suggests other physical mechanisms such as viscosity may play a role in size selection.

5.3 CONCLUSIONS

An investigation of data from various experiments performed during PLACES event JAN has been undertaken with the goal of determining the U-shaped curve parameter, R that best represents the data. Sources of data surveyed included the mass spectrometer (Narcisi et al., 1981) and electron density probe (Szuszczewicz et al., 1981) results from the rocket experiment, backpropagated aircraft data (Marshall et al., 1982) and photographic data provided by Wallace Boquist of Technology International Corporation.

As a first step in evaluating the appropriate M-ratio the barium and atomic ion mobility dependences on altitude is determined. From the mobility values and the mass spectrometer rocket measurements of ion density a value of 3.3 mho has been calculated in Section 2.2 to be the background height integrated Pedersen conductivity. The calculation accounts for the varying composition of ion and background constituents. It should be noted that the 3.3 mho value may be in error on the high side. Conservatively large values have been chosen for estimating the contribution of the background conductivity above the rocket trajectory. Also Linson (1984) indicates that the mass spectrometer density data (Figures 4 and 5) may be too large by a factor of 1.33.

As a second step in evaluating the M-ratio the barium cloud conductivity is estimated from aircraft total electron content measurements. Using a straightforward model of the propagation geometry and an estimate of the effective cloud altitude from the rocket data the cloud conductivity is estimated to be approximately 50 mhos in Section 2.3.

From the conductivities of the background and the barium cloud an M-ratio of 15 is deduced. Investigations of the coupling parameters implied by photographic measurements of cloud dynamics indicate an M-ratio of 3-5 is more appropriate. The discrepancy between the two values can be resolved if the coupling to the conjugate summer daytime ionosphere can enhance the background conductivity by 7 mhos. An analysis of the parallel-to-perpendicular conductivity ratio indicates that such coupling is possible if the driven structure is larger than 500 meters. Smaller structures probably do not couple to the enhanced conductivity of the conjugate region.

The preferred structure size suggested by JAN aircraft data is a 90 meter breakpoint scale or a 280 meter diameter. This value is fairly precise and is in acceptable agreement with photographic and rocket data which are less precise. Inherent difficulties associated with the measurement of the small distances corresponding to structure sizes limit the precision of the photographically determined value while the lack of an accurate value for the component of the rocket velocity transverse to the field limits the accuracy of the structure size from the density probe.

Steep density gradients, 18 meters per e-fold, are indicated by the JAN electron density probe data. These gradient lengths are comparable to though somewhat larger than those measured during the STRESS event ESTHER. An analysis of one structure in the JAN rocket data which has a steep gradient has been performed to estimate the magnitude and mechanisms of plasma cross-field diffusion. It is found that if the structure is assumed to have an ion-neutral slip speed of 17 meters per second then the magnitude of the diffusion coefficient is 3 meters squared per second. The diffusion rate appears to be independent of electron density suggesting electron-neutral collisions as the diffusion mechanism.

The measured wind speed of 50 meters per second, the structure size of 280 meters diameter, and the diffusion coefficient of 3 meters squared per second (at an ion-neutral slip speed of 17 meters per second) suggest that the U-shaped curve constant, R_k appropriate for outer scale dimensions is 220, while R_d, appropriate for diameters, is approximately 680 (Section 5). The value for, R, is fairly insensitive to the value of M which results from the analysis because the value of M enters into the U-shaped curve value $R((M-1/M+1)^2)$ in nearly the same manner that it enters into the value of LU/D

as determined by the data. This insensitivity is not surprising if it is accepted that the stability of a structure is dependent primarily upon the ratio of the two characteristic lengths in the problem, namely the size of the structure and the gradient length of its steepened front.

The value for R_d obtained from the JAN data is much larger than the value of R_d ($\approx$ 100) indicated by numerical simulation results. The discrepancy between the values appears to be significant since an error in stable structure sze, slip velocity or diffusion constant with a value of a factor of 6-7 must be found to dispel the discrepancy. It seems inconceivable that the largest stable size is amaller than 280 meters, and certainly not by a factor of two. Since the diffusion constant of $3m^2/s$ which results from the analysis is a high side estimate it seems difficult to accept that it is a factor of three or more too low. Thus, it appears reasonable to suggest that another size selection mechanism may be operative in JAN.

The seiving mechanism is offered as one possible selection mechanism. The mechanism stabilizes structure sizes that are too small to couple to conjugate region conductivity but that are larger than the stable size suggested by the coupled M-ratio. The problem with applying this mechanism to JAN data would be explaining the presence of such steep density gradients as those observed. The steepened density contours of uncoupled structures should be much more diffuse than the gradient measured in JAN if the ion-neutral slip were significantly decreased by seiving. It may be the case, however, that the structures which remain after seiving are fairly smooth and correspond to an unseeded numerical calculation. The ion neutral slip could still remain high which would maintain the steep gradients without necessitating bifurcation.

Yet another size selection mechanims which may be advanced to explain the JAN structure size data is ion-ion viscosity. Viscosity enters another length scale into the problem that could limit structure bifurcation and result in larger structure sizes.

LIST OF REFERENCES

1. Abramowitz, Milton A. and Irene A. Stegun, editors, Handbook of Mathematical Functions with Formulas, Graphs and Mathematical Tables, National Bureau of Standards, Applied Mathematics Series 55, 1970.
2. Banks, P.M. and G. Kocharts, Aeronomy, Academic Press, New York, 1973.
3. Brown, Sanford C., Basic Data of Plasma Physics, Cambridge, MIT Press, 1959.
4. Dupré, Robert Roussel, Los Alamos National Laboratory, private communication, June 1984.
5. Francis, Samuel H. and Francis W. Perkins, "Determination of Striation Scale Sizes for Plasma Clouds in the Ionosphere," Journal of Geophysical Research. vol. 82, no. 22, August 1, 1975, pp. 3111-3120.
6. Gonzalez, "FPS-85 radar operations" in D.R. McDaniel, compiler, Proceedings of the PLACES Preliminary Data Review Meeting, 20 and 21 May 1981, DNA 5848P, July 1981.
7. Hochstim, A.R., A.R. Howard Jr., "Code for Atmospheric and Transport Properties (CATP)," in R.S. Leonard and D.N. McDaniel, Project SECEDE--1970 Summer Study Proceedings, RADC TR-70-216, Vol. III.
8. Kilb, Ralph W., "Striation Formation," Chapter 13 in D.H. Holland et al. Physics of High Altitude Nuclear Burst Effects, Mission Research Corporation, DNA 4501F, December 1977.
9. Kilb, Ralph W., Mission Research Corporation, 6 July 1984(a) presentation to JASON.
10. Kilb, Ralph W., Mission Research Corporation, 14 September 1984(b), presentation to DNA late-time structure group.
11. Linson, L.M., "Phenomenological Predictions," in R.S. Leonard and D.N. McDaniel, Project SECEDE--1970 Summer Study Proceedings, RADC TR-70-216, Vol. III, 1970.

12. Linson, L.M., "Status of Theoretical Understanding of Barium-Ion-Cloud Phenomenology," in D.R. McDaniel, compiler, PROJECT SECEDE--Proceedings of the SECEDE II Final Data Review Meeting, RADC-TR-72-153, Vol II, May 1972.

13. Linson, L.M. and David C. Baxter, Ion Cloud Modelling, Defense Nuclear Agency Report DNA 4455F, 1977.

14. Linson, L.M. and David C. Baxter, STRESS Ion Cloud Modelling, SAI report number SAI-78-835-LJ, August 1978.

15. Marshall, J.M., J.W. Lehman, Gary Elston, and W.E, Solbrig, PLACES Quick-look Report for Beacon and Aircraft Experiments, Defense Nuclear Agency Report, DNA 5737F, March 1981.

16. Marshall, J.M., W.E. Solbrig, and J.W. Lehman, PLACES Aircraft Equipment Test Results, DNA-TR-81-233, May 1982.

17. McDonald, B.E., S.L. Ossakow, S.T. Zalesak, and N.J. Zabusky, "Scale Sizes and Lifetimes of F-Rgion Plasma Cloud Striations as Determined by the Condition of Marginal Stability," JGR, vol. 86, no. A7, pp. 5775-5784, July 1981.

18. Narcisi, R., E. Trzcinski, G. Federico, W. Wlodkya, and P. Bench, "Composition and Structure Measurements [,] Ionospheric Barium Cloud," in D.R. McDaniel, compiler, Proceedings of the PLACES Preliminary Data Review Meeting, 20 and 21 May 1981, DNA 5448P, July 1981.

19. Prettie, Clifford W., Results of PLACES Data Analysis, Defense Nuclear Agency Report, DNA-TR-81-170, 1982.

20. Simons, David J., Charles F. Lebeda, Morris B. Pongratz, T. Joseph Fitzgerald, and Robert Roussel-Dupré, Evolution of Structure in the PLACES Barium Clouds, Los Alamos National Laboratories report LA 9648-MS, February 1984.

21. Szuszczewicz, E.P., J.C. Holmes, C.S. Lin, and M. Swinney, "DNA PLACES Barium Event JAN" in D.R. McDaniel, compiler, Proceedings of the PLACES Preliminary Data Review Meeting, 20 and 21 May 1981, DNA 5448P, July 1981.

22. Zalesak, S.T. and J.D. Huba, "On the Linear Stability of Two Dimensional Barium Clouds, I. The Inviscid Case," Naval Research Laboratory Memorandum Report 5312, April 1984.

23. _____, U.S. Standard Atmosphere, 1976, U.S. Government Printing Office, NOAA-S/T76-1562, 1976.

DISTRIBUTION LIST

DEPARTMENT OF DEFENSE

Defense Intell Agency
ATTN: RTS-2B

Defense Nuclear Agency
ATTN: NATF
ATTN: NAWE
ATTN: RAAE, P. Lunn
ATTN: RAAE, K. Schwartz
ATTN: RAEE
ATTN: STNA
3 cys ATTN: RAAE
4 cys ATTN: STTI-CA

Defense Tech Info Ctr
12 cys ATTN: DD

DEPARTMENT OF THE ARMY

BMD Advanced Technology Center
ATTN: ATC-O, W. Davies
ATTN: ATC-R, D. Russ
ATTN: ATC-R, W. Dickinson
ATTN: BMDATC-D, M. Capps

US Army Nuc & Chem Agency
ATTN: Library

DEPARTMENT OF THE NAVY

Naval Ocean Systems Center
ATTN: Code 532
ATTN: Code 5322, M. Paulson
ATTN: Code 5323, J. Ferguson

Naval Research Laboratory
ATTN: Code 4108, P. Rodriguez
ATTN: Code 4187
ATTN: Code 4700
ATTN: Code 4700, S. Ossakow
ATTN: Code 4720, J. Davis
ATTN: Code 4780
ATTN: Code 6700
ATTN: Code 7500, B. Wald
ATTN: Code 7950, J. Goodman

DEPARTMENT OF THE AIR FORCE

Air Force Weapons Laboratory
ATTN: NTN
ATTN: SUL

Air Force Wright Aeronautical Lab/AAAD
ATTN: A. Johnson
ATTN: W. Hunt

Strategic Air Command
ATTN: SAC/SIJ
ATTN: NRI/STINFO
ATTN: SAC/SIZ
ATTN: XPFC
ATTN: XPQ

DEPARTMENT OF ENERGY

Los Alamos National Laboratory
ATTN: D. Sappenfield
ATTN: D. Simons
ATTN: G-6, E. Jones
ATTN: J. Wolcott
ATTN: MS 664, J. Zinn
ATTN: R. Jeffries
ATTN: T. Kunkle, ESS-5

DEPARTMENT OF DEFENSE CONTRACTORS

Autometric, Inc
ATTN: C. Lucas

BDM Corp
ATTN: L. Jacobs
ATTN: T. Neighbors

Berkeley Rsch Associates, Inc
ATTN: J. Workman
ATTN: S. Brecht
2 cys ATTN: C. Prettie

EOS Technologies, Inc
ATTN: B. Gabbard
ATTN: W. Lelevier

JAYCOR
ATTN: J. Sperling

Kaman Tempo
ATTN: B. Gambill
ATTN: DASIAC
ATTN: W. McNamara

Kaman Tempo
ATTN: DASIAC

MAXIM Technologies, Inc
ATTN: E. Tsui
ATTN: J. Marshall
ATTN: R. Morganstern

Mission Research Corp
ATTN: C. Lauer
ATTN: D. Knepp
ATTN: F. Fajen
ATTN: F. Guigliano
ATTN: G. McCartor
ATTN: R. Bigoni
ATTN: R. Bogusch
ATTN: R. Dana
ATTN: R. Hendrick
ATTN: R. Kilb
ATTN: S. Gutsche
ATTN: Tech Library

Mitre Corp
ATTN: A. Kymmel
ATTN: C. Callahan
ATTN: MS J104, M. Dresp

DEPARTMENT OF DEFENSE CONTRACTORS (Continued)

Pacific-Sierra Research Corp
ATTN: E. Field, Jr.
ATTN: F. Thomas
ATTN: H. Brode, Chairman SAGE

Pacifica Technology
ATTN: E. Giller

Photometrics, Inc
ATTN: I. Kofsky

Physical Dynamics, Inc
ATTN: E. Fremouw

Physical Research, Inc
ATTN: R. Deliberis
ATTN: T. Stephens

Physical Research, Inc
ATTN: J. DeVore
ATTN: J. Thompson
ATTN: K. Schlueter

R&D Associates
ATTN: B. Moller
ATTN: C. Greifinger
ATTN: F. Gilmore
ATTN: G. StCyr
ATTN: H. Ory
ATTN: M. Gantsweg
ATTN: M. Gover
ATTN: P. Haas
ATTN: R. Turco
ATTN: W. Karzas
ATTN: W. Wright

DEPARTMENT OF DEFENSE CONTRACTORS (Continued)

R&D Associates
ATTN: B. Yoon

R&D Associates
ATTN: G. Ganong

Science Applications Intl Corp
ATTN: C. Smith
ATTN: D. Hamlin
ATTN: E. Straker
ATTN: L. Linson

SRI International
ATTN: A. Burns
ATTN: C. Rino
ATTN: D. McDaniel
ATTN: D. Nielson
ATTN: G. Price
ATTN: G. Smith
ATTN: J. Petriceks
ATTN: J. Vickrey
ATTN: M. Baron
ATTN: R. Leadabrand
ATTN: R. Livingston
ATTN: R. Tsunoda
ATTN: V. Gonzalez
ATTN: W. Chesnut
ATTN: W. Jaye

Toyon Rsch Corp
ATTN: J. Garbarino
ATTN: J. Ise

VisiDyne, Inc
ATTN: J. Carpenter